

Accurate Split Learning on Noisy Signals

Anonymous authors

Paper under double-blind review

Abstract

Noise injection is applied in Split Learning to address privacy concerns about data leakage. Previous works protect Split Learning by adding noise to the intermediate results during the forward pass. Unfortunately, noisy signals significantly degrade the accuracy of Split Learning training. This paper focuses on improving the training accuracy of Split Learning over noisy signals while protecting training data from reconstruction attacks. We propose two denoising techniques, namely scaling and random masking. Our theoretical results show that both of our denoising techniques accurately estimate the intermediate variables during the forward pass of Split Learning. Moreover, our experiments with deep neural networks demonstrate that the proposed denoising approaches allow Split Learning to tolerate high noise levels while achieving almost the same accuracy as the noise-free baseline. Interestingly, we show that after applying our denoising techniques, the resultant network is more resilient against a state-of-the-art attack compared to the simple noise injection approach.

1 Introduction

Privacy concerns in various application domains, including finance, healthcare, and online commerce, limit the sharing of raw data required to train accurate deep neural networks (DNNs). Split Learning Gupta & Raskar (2018); Vepakomma et al. (2018a) has emerged as a solution that enables different parties to collaboratively learn a model, without explicitly sharing raw input data. Typically, in two-party Split Learning, the Split Neural Network (SplitNN) is divided between the *data owner*, a.k.a. the client, and the *label owner*, a.k.a. the server; see Figure 1 (a). During training, in the forward pass, the client forwards the intermediate results (IRs) (i.e., the neurons of the *cut layer*, the last layer in the client’s part of the DNN) to the server. The server completes the forward pass, and during the backpropagation, it returns the gradients of the IRs to the client. Consequently, the client can train the joint model without revealing the private training data to the server.

Unfortunately, sharing only the IRs does not protect the raw data. The shared IRs contain considerable latent information about the data and can be used to stage powerful attacks, such as model inversion attack He et al. (2019a); Zhang et al. (2020); Erdogan et al. (2021), label inference attack Erdogan et al. (2021); Kariyappa & Qureshi (2021); Li et al. (2021), and hijacking attack Pasquini et al. (2021). Several works Titcombe et al. (2021); Abuadbbba et al. (2020); Mireshghallah et al. (2020); Wang et al. (2018) attempt to mitigate that risk through adding a certain amount of noise to the IRs before sharing with the other party. However, one of the fundamental issues of adding noise is the trade-off between the trained model’s quality and its susceptibility to an external attacker. While high levels of noise are favorable in making the training data private, the noise inevitably impacts the quality of the trained model Abuadbbba et al. (2020); Wang et al. (2020a; 2021), that is, the accuracy; see Figures 1 (b) and (c) for an example. Thus, a fundamental question is: Can we improve the training accuracy of Split Learning under noise injection, without making the model vulnerable to data leakage?

We answer the above question affirmatively by applying a post-processing denoising layer on top of noise-injected IRs in the Split Learning process. Our intuition is that *the injected noise introduces an error during the forward pass, which is dominated by variance when the noise level is high*. As long as we can reduce the variance by using denoising techniques, the training quality should be improved. Such a post-processing layer

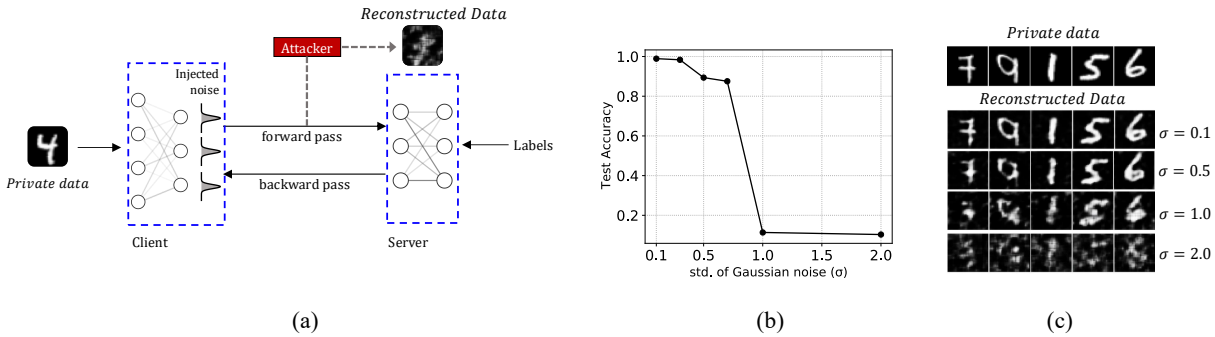


Figure 1: The trade-off between the security and training accuracy in noise-injected private Split Learning. (a) General schematic representation of two-party split learning, where the neural network is split between the client (owns the data) and server (owns the labels). Noise is injected at the client’s side output to prevent private data leakage from the attacker. (b) Noise variance (σ) vs. Test accuracy in training a split CNN model on the MNIST dataset. As the variance of the injected noise level (σ) increases, the test accuracy drops. (c) Training data reconstruction by hijacking attack at different injected noise levels. The reconstruction capacity decreases as the injected noise level is increased.

will not impose any additional private information leakage as long as it does not interact with the original private data.

We list our contributions as follows:

Contributions. (i) We propose two denoising techniques (i.e., scaling and masking) to improve the training accuracy and stability of noise-injected SplitNN; see §3. (ii) Our theoretical investigation on a classification task in §3.2 shows that denoising can reduce the error caused by noise injection during the forward pass. (iii) In addition to improving the train model quality, we show that our modification to Split Learning with noise injection, followed by postprocessing, preserves the security guarantee in the entire training protocol; see §3.3. Quantifying the privacy aspect in our work is not the primary focus; it is an additional benefit. (iv) We validate our claims through extensive numerical experiments on synthetic and real data (i.e., 7 DNN models on 7 different datasets, including large-scale datasets, ImageNet1K Deng et al. (2009) and Amazon Reviews McAuley & Leskovec (2013)) in §4. Moreover, (v) we find that our masking technique, in addition to denoising, also enhances the resilience of Split Learning against the state-of-the-art hijacking attack Pasquini et al. (2021); refer to §4.3.

2 Related Work

Federated Learning (FL) with noise injection. Noise injection in vertical FL shares some similarities with noise-injected SplitNN, since in both cases, the noise is injected into intermediate results during the forward pass. Existing works Wang et al. (2020b); Chen et al. (2020) propose to add Gaussian/Laplacian noise on participants’ IRs to protect private training data or labels. Chen et al. (2020) only demonstrates the impact on training accuracy when some applications have a relatively low noise scale. The other framework Wang et al. (2020b) proposes a similar noise injection technique only for linear model collaborative learning, which is not directly applicable to general DNNs.

Split Learning with noise injection. Due to the vulnerability of SplitNN against model inversion attacks, Titcombe et al. (2021) proposed to apply differentially private noise injection on IRs during inference time to prevent data reconstruction by the attacker. Shredder, proposed by Mireshghallah et al. (2020), adaptively generates a noise mask to minimize mutual information between input and intermediate data. However, these two methods only introduce noise injection during the inference time; thus, the privacy of training data is not preserved. Abuadba et al. (2020) successfully applies noise to the IRs during the training to defend against model inversion attacks on one-dimensional ECG data; also, see Wu et al. (2023) for SpiltNN with differential privacy for integrated terrestrial and non-terrestrial Networks. It turns out that the noise has

dramatically impacted the model’s accuracy. Unlike previous works that only focus on the attack defense efficacy, we aim to improve the training accuracy with a significant noise level.

We provide an answer to split learning denoising by proposing two post-processing techniques (i.e., scaling and masking) to improve the accuracy and stability of the splitNN training when Gaussian noise is injected into the IRs. To our knowledge, we are the first to propose denoising techniques on the Gaussian noise-injected IRs to improve the training accuracy of SplitNN and theoretically show the privacy guarantee in this setup. In the following, for completeness, we mention some differential privacy (DP) techniques used in federated learning (FL) and related settings Bergou et al. (2023); Sun et al. (2024); Xu et al. (2021) for completeness.

Gaussian noise injections (GNIs) are a family of regularization methods for DNN training through adding Gaussian noise on the activations or weights during the forward pass. It is similar to the noise injection in SplitNN except for the following two aspects: (i) There is no requirement of bounded sensitivity in injection objects. (ii) The noise scale is usually set small to avoid negative impacts on training accuracy. The explicit regularization effects of GNIs are well investigated in Camuto et al. (2020); Li & Liu (2020); Lim et al. (2021), demonstrating better generalization for trained models over unseen data. In addition, GNIs can improve the robustness of DNNs against adversarial attacks or data perturbations Lim et al. (2021); He et al. (2019b). However, Camuto et al. (2021) also found that GNIs can introduce some implicit bias on gradient updates, which inevitably degrades the training accuracy.

Denoising. Adding the Gaussian noise and the denoising mechanisms in our work shares many similarities with the differential privacy (DP) and their post-processing that maintains the DP guarantee and often improves accuracy Zhu et al. (2022; 2021). Denoising for DP has been well adopted in the statistical estimation Hay et al. (2009; 2010); Nikolov et al. (2013); Bernstein et al. (2017), where they exploit some prior knowledge to design a data release mechanism with better DP utility. Recently, Balle & Wang (2018) proposed an optimal denoising technique for Gaussian mechanism, where given $y \sim \mathcal{N}(f(x), \sigma^2 I)$ and their target is to find a postprocessing function g such that $g(y)$ is closer to $f(x)$ than y . This is substantially different from SplitNN as there are subsequent layers on top of the Gaussian mechanism in the training process. Nasr & Shokri (2020) has also investigated using scaling as a denoising technique to improve the DP utility for DP-SGD Abadi et al. (2016). However, the authors scale up/down the noisy gradients based on the “usefulness” of gradients, while we utilize scaling to minimize the estimation error of the noisy neural network outputs. Wang et al. (2020a) showed that adding Laplacian smoothing on Gaussian noise-injected gradients can improve the utility of DP-SGD. While Ligett et al. (2017) proposed a general noise reduction framework, Lecuyer et al. (2019) proposed PiXel-DP, an adversarial defense mechanism, scalable to diverse large networks and datasets.

3 Theoretical Guarantee

Notations. By $[n]$ we denote the set of n natural numbers $\{1, 2, \dots, n\}$. By x_i , we denote the i^{th} component of vector x , while A_{ij} denote the $(i, j)^{\text{th}}$ component of a matrix, A . We use $\|x\|_2$ and $\|A\|_F$ to denote the ℓ_2 and the Frobenius norms of a vector x and a matrix A , respectively.

Problem setup. Let D be the training dataset with N elements, $\{(X_i, y_i^*)\}_{i=1}^N$, drawn i.i.d. from some distribution, $P(\mathcal{X}, \mathcal{Y})$, where $X_i \in \mathbb{R}^d$ is the input feature vector, and y_i^* is the corresponding ground-truth label. We consider a SplitNN with an output vector in \mathbb{R}^m . The network is divided between the client and the server, where the server network consists of several DNN layers and the output loss function. In our experiments, we show different split configurations; however, in our theoretical analysis, we have one fully connected (FC) layer after the cut layer as the final layer.

Let $X \in \mathbb{R}^n$ be the vector from the client-side cut layer, and $M \in \mathbb{R}^{m \times n}$ be the weight matrix of the FC layer on the server side. At each iteration during training, the original split network processes a minibatch of training samples to calculate the loss and, during backpropagation, updates the gradients. We follow this formalization in our theoretical analysis.

We consider the GNIs to protect the vector X . For Laplacian noise, see §B.1. Let the perturbed vector, $\tilde{X} \in \mathbb{R}^n$ follow the model: $\tilde{X} = X + Z$, where $Z_i \sim \mathcal{N}(0, \sigma^2)$, chosen from a zero mean Gaussian distribution

with standard deviation $\sigma \in \mathbb{R}^+$. Then, we apply a post-processing function $h_D(\cdot) : \mathbb{R}^n \rightarrow \mathbb{R}^n$ on \tilde{X} before forwarding it to the server side. To bound the magnitude of X , we use \tanh as the activation function.

If we set the cut layer at an arbitrary i -th layer in an L -layer DNN, along with the final loss function used for DNN training, the theoretical analysis would become less tractable. Therefore, in our setup, we set $i = L - 1$ to illustrate the main ideas. We formalize two possible cases in the forward pass to the output layer: (i) a linear layer, $\Phi = I_m$, an identity map, and we quantify $\mathbb{E}\|MX - Mh_D(\tilde{X})\|_2^2$ against $\mathbb{E}\|MX - M\tilde{X}\|_2^2$; see §3.1, and (ii) a linear layer with a nonlinear activation function (Softmax), $\Phi = s$, nonlinear loss function (negative log), \mathcal{L}_{LL} , and we quantify $\mathbb{E}|\mathcal{L}_{LL}(y^*, s(MX)) - \mathcal{L}_{LL}(y^*, s(Mh_D(\tilde{X})))|$ against $\mathbb{E}|\mathcal{L}_{LL}(y^*, s(MX)) - \mathcal{L}_{LL}(y^*, s(M\tilde{X}))|$, where y^* is the true label vector; see §3.2. In both cases, h_D is a post-processing mechanism that is used to improve the training quality, resulting in some “denoising” effect; the signal-to-noise ratio is not the measure of “denoising” in our context.

Our primary focus is on nonlinear classification tasks, although for a better understanding, denoising the linear layer is important, which can be viewed as a regression task. Our theorems are proxies to measure whether the postprocessing would allow better server accuracy. We do not include an iteration counter on M, X , or \tilde{X} ; we are examining the single forward pass. We use a random masking operator, R_p , and a scaling operator, S_α , as h_D , defined below:

(i) **Random masking operator.** Let R_p be a random matrix of 1’s and 0’s with identical and independently distributed entries, $(R_p)_{ij} \sim \text{Bernoulli}(p)$. Denote the support set, $\Omega_p \subset [m] \times [n]$ of R_p as $\Omega_p := \{(i, j) | (R_p)_{ij} = 1\}$. Based on this, for a matrix, $A \in \mathbb{R}^{m \times n}$,

$$(R_p[A])_{ij} = \begin{cases} A_{ij} & : i \in \Omega_p, \\ 0 & : \text{otherwise.} \end{cases}$$

From the definition, R_p is linear and is a projection operator, that is, $R_p^2 = R_p$.

(ii) **Scaling operator.** For a matrix $A \in \mathbb{R}^{m \times n}$ and $\alpha > 1$, denote the element-wise scaling operator, $S_\alpha(\cdot) : \mathbb{R}^{m \times n} \rightarrow \mathbb{R}^{m \times n}$, as $S_\alpha(A) = \frac{1}{\alpha}A$. Unlike the random masking, the scaling operator, S_α has no randomness.

3.1 A linear layer

With the above setup, to easily explain our ideas, we start with a neural network performing simple regression. Although this is not our primary focus, we believe this section provides a better understanding in a simple setting. Because for the ℓ_2 -regression task, no nonlinear activation function is required, the problem is much simpler. That is, $y := MX$ is the prediction of the output layer, and it does not involve any non-linearity. Theorem 3.1 describes results for a fully-connected DNN with an ℓ_2 -regression task. Additionally, it explains how the scaling and masking parameters, α and p , respectively, are related to the noise scale σ , while denoising the output of a linear layer of a DNN for a given M and X . We calculate the expected test error, $\mathbb{E}\|MX - Mh_D(\tilde{X})\|_2^2$, where h_D is R_p or S_α , and compare it against $\mathbb{E}\|MX - M\tilde{X}\|_2^2$.

Next, we will prove Theorem 3.1, for ℓ_2 -regression task; See §A.2 for the proof. For Theorem 3.1, the prediction of the DNN model does not involve any nonlinearity. Throughout Sections 3.1 and 3.2, $\mathbb{E}_p(\cdot | \tilde{X})$ denotes expectation conditioned on the randomness in R_p given \tilde{X} , and $\mathbb{E}_Z(\cdot)$ denotes expectation taken on the randomness in \tilde{X} .

Theorem 3.1. *With the notations above, we have (i) $\mathbb{E}\|MX - MR_p(\tilde{X})\|_2^2 \leq \mathbb{E}\|MX - M\tilde{X}\|_2^2$ if and only if $p\|M \odot \tilde{X}\|_F^2 + (1 - p)\|MX\|_2^2 \leq \sigma^2\|M\|_F^2$, where $\tilde{X} \in \mathbb{R}^{m \times n}$ is a matrix obtained by stacking $X^\top \in \mathbb{R}^{1 \times n}$ in each row, and \odot denotes the elementwise product. (ii) Let $\alpha > 1$. $\mathbb{E}\|MX - MS_\alpha(\tilde{X})\|_2^2 \leq \mathbb{E}\|MX - M\tilde{X}\|_2^2$ if and only if $\frac{\|MX\|_2^2}{\|M\|_F^2} \leq \left(\frac{\alpha+1}{\alpha-1}\right)\sigma^2$.*

Remark 3.2. Theorem 3.1 considers the most commonly used mean square error (MSE), $\mathbb{E}\|MX - MR_p(\tilde{X})\|_2^2$ and $\mathbb{E}\|MX - MS_\alpha(\tilde{X})\|_2^2$, respectively, to compare against $\mathbb{E}\|MX - M\tilde{X}\|_2^2$. We use the MSE because it has nice mathematical properties; one can use other loss functions. This MSE is agnostic of the nature of the loss function used in DNN training.

Remark 3.3. Since the expected MSE can be decomposed into bias and variance, by showing the relation between the expected MSEs as in Theorem 3.1, the bias-variance trade-off between different processes can be explained.

3.2 Nonlinear loss function for classification task

For a vector, $z \in \mathbb{R}^m$, denote $s : \mathbb{R}^m \rightarrow (0, 1)^m$ as the softmax function, and $\mathcal{L}_{LL}(y^*, s(z))$ as the negative log loss function, where y^* is the true label vector; see definition in §A.1. In what follows, we show that for both masking and scaling operators, under certain conditions on the noise level, σ , it is possible to find parameters p and α , respectively, such that, by using any of these operations, we incur a lower deviation in the loss value than using the noise injection alone when compared to the loss of the original SplitNN.

Masking operation. Quantifying $\mathcal{L}_{LL}(y^*, s(MR_p(\tilde{X})))$ and $\mathcal{L}_{LL}(y^*, s(M\tilde{X}))$ are critical as they involve randomness from the masking operator and the Gaussian noise. We require several intermediate results to prove the main result in Theorem 3.4. We state and prove them in the § A.3.1.

We want to show that by using a random mask over a noise-injected layer, we incur a lower deviation in the loss value than using the noise injection alone when compared to the loss, $\mathcal{L}_{LL}(y^*, s(MX))$, of the original SplitNN under certain conditions. That is, we want to compare the quantities $\mathbb{E}|\mathcal{L}_{LL}(y^*, s(MX)) - \mathcal{L}_{LL}(y^*, s(MR_p(\tilde{X})))|$ and $\mathbb{E}|\mathcal{L}_{LL}(y^*, s(MX)) - \mathcal{L}_{LL}(y^*, s(M\tilde{X}))|$. The following result formalizes this.

Theorem 3.4. *With the notations above, for classification problems, assume that $n \geq (MX)_i$ for $i = 1, 2, \dots, m$ and let the higher order moments, $m_p = \mathbb{E}|\sum_{i=1}^m e^{(MR_p(\tilde{X}))_i} - \mathbb{E}(\sum_{i=1}^m e^{(MR_p(\tilde{X}))_i})|^p$ be small for $p = 2, 3, \dots$. Then, if σ is large enough, there is some $\delta \in (0, 1)$ such that for $p \in (\delta, 1]$,*

$$\mathbb{E}|\mathcal{L}_{LL}(y^*, s(MX)) - \mathcal{L}_{LL}(y^*, s(MR_p(\tilde{X})))| \leq \mathbb{E}|\mathcal{L}_{LL}(y^*, s(MX)) - \mathcal{L}_{LL}(y^*, s(M\tilde{X}))|.$$

The assumption, $n \geq (MX)_i$ is technical and can be easily satisfied in practice, which requires the input dimension from the SplitNN to be wide enough. We will pause here and provide a sketch of proof of Theorem 3.4. Because the original SplitNN always produces the least loss, the expressions in absolute values in the inequality above are non-positive, and so we need only to verify that for all X , $\mathbb{E}\mathcal{L}_{LL}(y^*, s(MX)) - \mathcal{L}_{LL}(y^*, s(M\tilde{X})) \leq \mathbb{E}\mathcal{L}_{LL}(y^*, s(MX)) - \mathcal{L}_{LL}(y^*, s(MR_p(\tilde{X})))$. By the definitions of softmax and negative log loss, we have

$$\mathcal{L}_{LL}(y^*, s(MR_p(\tilde{X}))) = -(MR_p(\tilde{X}))_{i^*} + \log \left(\sum_{i=1}^m e^{(MR_p(\tilde{X}))_i} \right), \quad (1)$$

where i^* is the location of true label in y^* . For fixed M and \tilde{X} , (1) is a function of p for $p \in (0, 1]$. Denote $\mathcal{F}(p) := \mathbb{E}\mathcal{L}_{LL}(y^*, s(MR_p(\tilde{X})))$, and consequently, $\mathcal{F}(1) = \mathbb{E}\mathcal{L}_{LL}(y^*, s(M\tilde{X}))$; see Remark A.3. By using Lemma A.4 on (1), we can approximate $\mathcal{F}(p)$ by

$$\mathcal{F}(p) \approx -p(MX)_i + \log \left(\mathbb{E} \sum_{i=1}^m e^{(MR_p(\tilde{X}))_i} \right) - \frac{\text{Var} \left(\sum_{i=1}^m e^{(MR_p(\tilde{X}))_i} \right)}{2 \left(\mathbb{E} \left(\sum_{i=1}^m e^{(MR_p(\tilde{X}))_i} \right) \right)^2}. \quad (2)$$

We want to show that $\mathcal{F}(p) \leq \mathcal{F}(1)$ when $p \in (\delta, 1)$, for some $\delta \geq 0$. By using Lemma A.2 in (2) and differentiating with respect to p , we can show, $\mathcal{F}'(1) \geq 0$. This would imply that $\mathcal{F}(p)$ is an increasing function of $p \in (\delta, 1]$, for some $\delta \in (0, 1)$. This gives us $\mathbb{E}\mathcal{L}_{LL}(y^*, s(MR_p(\tilde{X}))) \leq \mathbb{E}\mathcal{L}_{LL}(y^*, s(M\tilde{X}))$, and §A.3.1 concludes the proof of Theorem 3.4.

Scaling operation. Similarly, by using scaling over \tilde{X} , under certain conditions on the noise level, σ , we obtain a lower deviation in the loss than using the noise injection alone when compared to the loss of the original SplitNN. Let $\tilde{\mathcal{L}}_{S_\alpha} := \mathcal{L}_{LL}(y^*, s(MS_\alpha(\tilde{X})))$. We state the result in Theorem 3.5; see §A.3.2 for a sketch of the proof.

Theorem 3.5. *With the notations above, for classification problems, if $\sigma^2 \geq \max_{i,i^*} \frac{\sum_{k=1}^n (m_{i^*k} - m_{ik})x_k}{\sum_{k=1}^n m_{ik}^2}$, for $i = 1, 2, \dots, m$, then there exists a $\delta' \in (0, 1)$ such that $\mathbb{E}|\mathcal{L}_{LL}(y^*, s(MX)) - \tilde{\mathcal{L}}_{S_\alpha}| \leq \mathbb{E}|\mathcal{L}_{LL}(y^*, s(MX)) - \mathcal{L}_{LL}(y^*, s(M\tilde{X}))|$, for $\alpha \in (1, \frac{1}{\delta'}]$.*

For concentration of the errors in Theorem 3.1 and Theorem 3.4; see §A.3.3.

3.3 Differential privacy (DP) preservation

Recent works show that Split Learning with Laplacian or Gaussian noise injection at the cut layer is resilient to attacks Abuadbbba et al. (2020); Wu et al. (2023). In particular, DP (see Definition in §A.4) could be used to describe the privacy guarantee. In this sub-section, we explain how our modification (scaling or masking) to Split Learning with noise injection (such as GNI) preserves DP. The key to our argument is to view our modification as a post-processing of a DP mechanism. Then, by the immunity of DP to post-processing, we can conclude that DP will be preserved.

Next, in light of our results in §3.1 and §3.2, we recall some terminologies needed for our discussion. For more details, see Dwork et al. (2014); Xiang et al. (2019); Abadi et al. (2016).

Let \mathcal{D} be a collection of databases. $D \in \mathcal{D}$ and $D' \in \mathcal{D}$ be two neighboring training datasets, that is, $D' = D \pm \{X\}$. In this case, we write $d(D', D) = 1$. For a function $V : \mathcal{D} \rightarrow \mathbb{R}^m$, define a randomized mechanism, $\mathcal{K} : \mathcal{D} \rightarrow \mathcal{O}$ such that, for $D \in \mathcal{D}$,

$$\mathcal{K}(D) := V(D) + Z, \quad (3)$$

where $Z \in \mathbb{R}^m$ is a random variable/vector with probability density function, $p(z)$.

To ensure \mathcal{K} is (ϵ, δ) -DP, one must require some condition on the density function $p(z)$ of Z . For example, if $p(z)$ is Laplacian or Gaussian density functions with their variances satisfying some lower bounds, then \mathcal{K} is DP. But, before we recall the result, we need one more important concept.

Define the *sensitivity* of V as

$$\Delta := \sup_{D, D', d(D, D')=1} \|V(D) - V(D')\|_2. \quad (4)$$

The following Theorem by Dwork et al. (2014) says, in the case when $m = 1$, if $z \sim \mathcal{N}(0, \sigma^2)$, then the random mechanism \mathcal{K} , as defined in (3) is DP as long as σ is large enough.

Theorem 3.6. (Dwork et al., 2014, Theorem 3.22) *Let $\epsilon \in (0, 1)$ be arbitrary. For $c^2 > 2 \ln(1.25/\delta)$, the mechanism in (3) with parameter $\sigma \geq c\Delta/\epsilon$ is (ϵ, δ) -differentially private.*

In Theorem 3.6, we note that the noise level σ is directly proportional to the sensitivity Δ and inversely proportional to the privacy bound ϵ .

This result will give us the DP of GNI for Split Learning (Lecuyer et al., 2019, §III.B), which suggested putting the cut layer early in the network, where bounding the sensitivity is easier. The next result allows us to see that both scaling and masking proposed in this work will preserve DP.

Theorem 3.7. (Dwork et al., 2014, Proposition 2.1) *Let \mathcal{K} be a randomized mechanism which is (ϵ, δ) -DP. If $g : \mathbb{R}^m \rightarrow \mathbb{R}^d$ is a deterministic or randomized mapping, then $g \circ \mathcal{K}$ is also (ϵ, δ) -DP.*

Impact on backpropagation. Now, we discuss the induced change during the backpropagation. In DNN training, backpropagation is used to evaluate the gradients, which will be used to update the estimation of parameters. As the popular DP procedure applied to DNN is DP-SGD Abadi et al. (2016), we indicate how our scaling and masking would “alter” the gradients that could be viewed as an approximate DP-SGD. Let g^t be the gradient and g_C^t denote the clipped version of g^t during the t -th iteration. DP-SGD would add Gaussian noise $Z \sim \mathcal{N}(0, \sigma I)$ to g_C^t . What happened to our case is that starting from the beginning of the backpropagation, we will evaluate gradients at the “perturbed” values (due to the GNI and our modification using scaling or masking from the cut layer) and these values will be used to propagate backward at each layer to obtain \tilde{g}_C^t , a perturbed version of g^t and hence g_C^t . Thus, we can put this into the framework of (3) with $\mathcal{K}(D) = \tilde{g}_C^t(D)$, $V(D) = g_C^t(D)$, and write

$$\tilde{g}_C^t(D) = g_C^t(D) + Z,$$

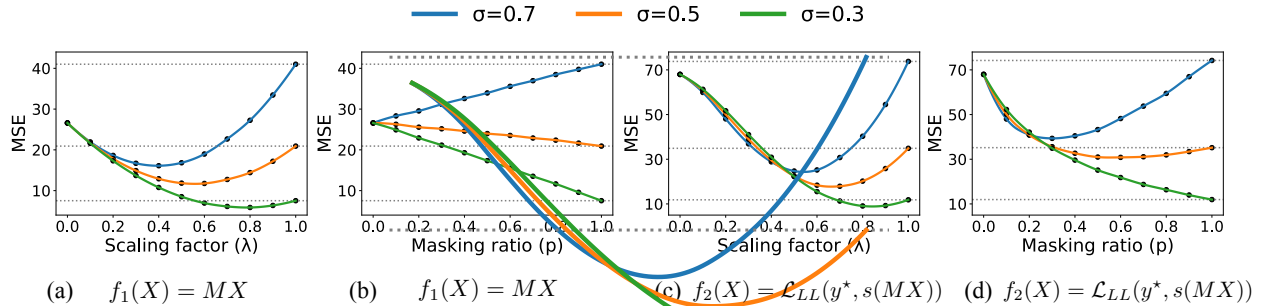


Figure 2: Simulation of how scaling factor ($\lambda = \frac{1}{\alpha}$) and masking ratio (p) influence the estimation error (MSE) under different noise levels (σ) for linear (f_1) and nonlinear functions (f_2, f'_2).

where Z is a random variable/vector due to the randomness of GNI and masking (using Bernoulli distribution). Although Z itself may not be Gaussian, it can be shown that $Z = g(W)$ where g is a sum of products of compositions of affine transformations and activation functions, and W is a random vector of independent Gaussian and Bernoulli variables. Let $p(z)$ denote the “density” of Z . Denote the sensitivity of $g_C^t(\cdot)$ by Δ_g . Define

$$S = \{w : p(w) > e^\epsilon p(w + \Delta_g)\}.$$

We can establish the following theorem, whose proof is given in the §A.10.

Theorem 3.8. *Let $\delta > 0$ and recall that Z is a random variable with probability density $p(z)$. Then, there exists an $\alpha > 0$ such that, for $\Delta_g \leq \alpha$,*

$$\Pr(Z \in S) < \delta,$$

where $P[\cdot]$ refers to the probability associated with the random variable. Furthermore, when $\Delta_g \leq \alpha$, \tilde{g}_C^t is (ϵ, δ) -DP.

Remark 3.9. Let D and D' be any pair of large training datasets with a single-entry difference, and without loss of generality, we have $D = D' \cup d$. Since $|D| = n$ is large for a large dataset, the empirical risk minimization function (a.k.a. loss function), \mathcal{L} will follow the relation: $\frac{1}{n}\mathcal{L}(D, Y) = \frac{1}{n}\mathcal{L}(D', Y) + \frac{1}{n}\mathcal{L}(d, y) \approx \frac{1}{n}\mathcal{L}(D', Y)$, where Y denotes the ground-truth label. Consequently, we can claim that, during backpropagation, Δ_g is small for large datasets (i.e., when $|D|$ is large), based on the definition of sensitivity. Thus, we can make the sensitivity small by requiring large training datasets, and we can claim that Δ_g is small for large datasets.

The above explains DP in one iteration of the training data. If we consider a total of T training iterations, we can use the advanced composition theorem, Theorem A.7 to guarantee, the mechanism is $(\epsilon\sqrt{2T\ln(1/\delta')} + T\epsilon(e^\epsilon - 1), T\delta + \delta')$ -DP for all $\delta' > 0$.

We can give a similar guarantee when the noise mechanism is Laplace. Also, note that, if in each training iteration, $g_{C,B}^t$ represents the clipped gradient calculated over a minibatch of size B taken from large enough databases, then for sensitivity, $\Delta_{g,B}$ small enough, the DP guarantee for $g_{C,B}^t$ holds following the same argument as above; see Xiang et al. (2019), and our discussion in §A.4.

In our experiments, we use the regular backpropagation formula for our noisy split network training; see Proposition A.8. Noise injection and postprocessing in the forward pass perturb the gradients during the backward pass, but without adding any explicit noise to them in each iteration. However, this is not the same as GNIs to the gradient as in DP-SGD Abadi et al. (2016)—The noise, in our case, (i) is a more general, data-adapted random variable than Gaussian, and that (ii) it is generated over the DNN architecture, not a user-specified Gaussian noise.

4 Experimental Evaluation

In §4.1, we validate our theoretical claims through simulation on synthetic data, §4.2 shows results on DNNs performing machine learning tasks, and Section §4.3 shows improved data privacy results.

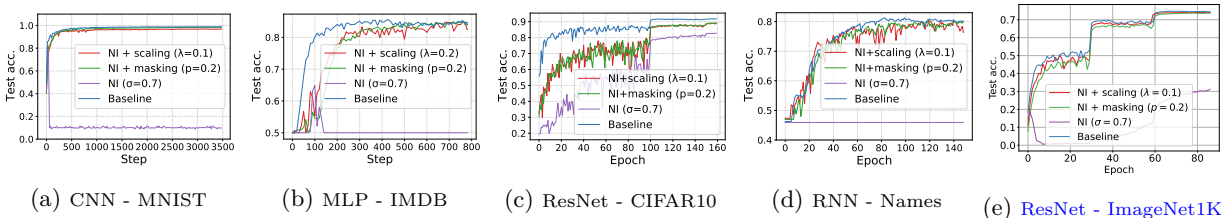


Figure 3: Test accuracy of [the best run for SplitNN training with noise injection \(NI\) only and noise injection \(NI\) plus denoising \(i.e. masking or scaling\)](#) in different training tasks. All models are split with one FC layer on the server side (σ : noise level, p : masking ratio, λ : scaling factor $\frac{1}{\alpha}$).

4.1 Simulation

Setup. The following numerical simulations verify the results of Theorem 3.1 and 3.4. Since $X \in [-1, 1]$ is the output of \tanh function, and M is usually randomly initialized around 0 in the actual training, we sample the entries of X and M from a uniform distribution on $[-1, 1]$ in our simulation. The MSE of masking corresponds to $\mathbb{E}\|f(X) - f(R_p(\tilde{X}))\|_2^2$ for all different functions (f_1, f_2, f'_2 in Figure 2), where R_p can be replaced by S_α for scaling. Moreover, when $p = 1$ and $\lambda = \frac{1}{\alpha} = 1$, masking and scaling are ineffective thus the respective MSEs are considered baseline MSEs. In Figure 2, for each plot, we draw a line parallel to the X-axis from these baseline MSEs. The expectations are calculated by taking the average on k simulation results, where $k = 1000$.

Scaling simulation. In Figure 2 (a), each curve corresponds to a different noise scale, σ . By decreasing the scaling factor, λ for each σ , the MSE first decreases from the baseline to a minimum then increases, indicating an optimal λ for each σ . The NASC condition in Theorem 3.1 (ii) also infers that. For fixed M, X , this condition implies it is possible to find a smaller λ when σ is large. We make similar observations for the nonlinear case; see Figure 2 (c).

Masking simulation. Figure 2 (b) shows that by decreasing the masking ratio, p , the MSE does not necessarily become smaller unless σ is large enough. This verifies the claim of Theorem 3.1(i). More importantly, there is an *almost linear* relationship between MSE and the masking ratio as $p \rightarrow 1$. This coincides with the expression of MSE with masking given in equation 9; see Appendix. We hypothesize that while both X, M are drawn from Uniform distribution, the coefficient of p^2 might become negligible. Hence, the coefficient of the linear term, p , which can be positive or negative depending on the noise scale σ , dominates the MSE. Results from Figure 2(d), with the nonlinear loss, reflect Theorem 3.4: σ^2 must be large for the *improvement to be possible*. If σ is too small (MSE curve for $\sigma = 0.3$), the masking does not work; the larger the σ , the more improvements one can expect by using masking. Moreover, when σ is large enough, there exists an $p \in (\delta, 1)$, for some $\delta \geq 0$ such that masking incurs a lower MSE than the baseline. This indicates that optimal denoising is possible by using masking for large noise. Nevertheless, for the same noise level, the MSE of the optimal denoising of masking is always larger than that of scaling. We provide the backward pass simulations in Figure 6 in §B. Figure 7 shows the simulation results for the Laplace mechanism, and they are discussed in detail in §B.1 along with experimental results in Table 3.

Takeaway message. Figures 2 (a), (c), and 6 (a) indicate that regardless of the noise scale, σ , it is possible to find a scaling factor such that using scaling over a noise-injected SplitNN incurs a lower MSE than the baseline. However, this is not always the case for the masking operator— σ must be significant for rendering the improvement. In practice, we witness masking performs better than scaling in terms of improved accuracy, parameter-tuning, and attack defense; see §4.2 and 4.3.

4.2 DNN Experiments

Datasets and models. We adopt the benchmarks from the popular Pytorch library Opacus Yousefpour et al. (2021) with the Split Learning paradigm. It contains image classification tasks (on MNIST LeCun et al.

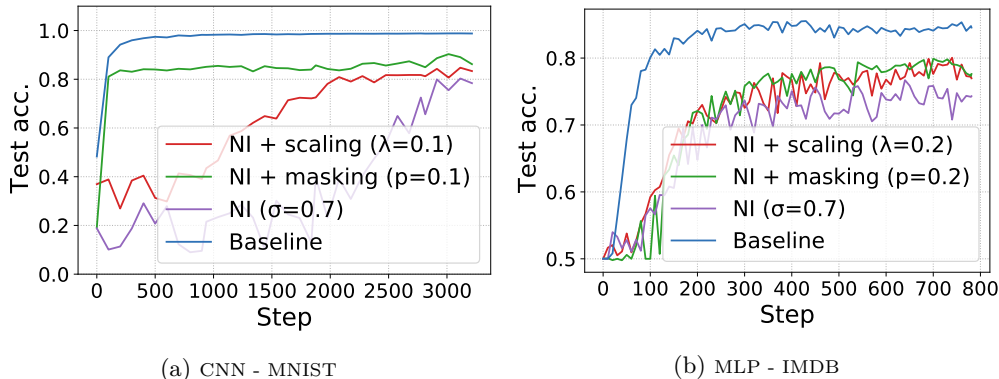


Figure 4: Test accuracy of SplitNN training with noise injection (NI) only and noise injection (NI) plus denoising (i.e. masking or scaling) with large split layer size and more than one layer at the server end; (a) CNN on MNIST, (b) MLP on IMDB.

(1998), CIFAR-10, CIFAR-100 Krizhevsky et al. (2009), and ImageNet1K Deng et al. (2009)), recommendation task (movie review prediction on IMDB Maas et al. (2011)), language modeling task (name classification Robertson (2023)), and sentiment analysis (Amazon reviews McAuley & Leskovec (2013)). All training hyperparameters are configured as default to maintain a fair comparison; see Table 2 in §B.

Setup and implementation. We split the models before fully connected (FC) layers, with a variety in the number of FC layers allocated at the server side; see Table 1. The size of the split layer varies from 16 to 12544. We use `tanh` activation function to bound the client’s output in $[-1, 1]$. Then, Gaussian noise is injected on the `tanh` layer, with noise scale, σ , the standard deviation of the Gaussian distribution. We implement both denoising techniques as a post-processing layer on top of the noise injection process. The ratio $p \in (0, 1)$ describes the percentage of the elements kept through masking. The scaling factor $\lambda = \frac{1}{\alpha} \in (0, 1)$ is used to scale down the tensor values. We have performed three runs for CNN-MNIST, MLP-IMDB, ResNet-CIFAR10, and LSTM-Names configurations and a single run for the rest of the configurations. The overall computation paradigm is outlined in Table 9 in §B.6.

Denoising performance. We demonstrate the effectiveness of the denoising techniques in various SplitNN training tasks. In Figure 3 and 4, we compare baseline SplitNN, noise-injected SplitNN, and noise-injected SplitNN with the scaling or masking denoising in 2 different split settings. The noise level, σ , is calibrated to a relatively high level such that the training accuracy of SplitNN suffers from the noise injection. Both scaling and masking are optimized by parameter tuning on the scaling factor, λ , and masking ratio, p ; see Table 10 in §B. When models are split at the last FC layer, e.g., in Figure 3 (a)(b)(d), once we inject a large noise ($\sigma = 0.7$), the overall training convergence is severely impacted so that the test accuracy is barely increased during the training. In Figure 4, the training is more robust under high noise injection because the size of the splitting layer is much larger than the one in previous settings. Usually, high-dimensional data can better tolerate noise perturbation since it carries more information. After applying the scaling or masking and fine-tuning some hyperparameters, the training convergence vastly improves. In most cases, e.g., Figure 3(a)(b)(d), the improved accuracy due to masking is comparable with the baseline. However, in Figure 4, with scaling and masking, the test accuracy can not achieve the baseline level. This is possible because, by allocating more layers on the server side, the client’s noisy IRs will also impact more layers during the forward computation. We also notice that in Figure 3 (c), the noise injected training on CIFAR-10 performs much better than other tasks, even though the split layer size is relatively small. This is due to its unique default parameter setup, such as weight decay and learning rate, which we will explain next.

Denoising vs. Hyperparameter tuning. To better understand the difference between denoising and traditional hyperparameter tuning, we evaluate the MNIST image classification task by fine-tuning the learning rate (lr), weight decay, dropout, masking ratio, and scaling factor under high-level noise injection. We present the accuracy results in §B in Table 4. Full training curves are available in §B in Figure 8. We change the lr from 0.1 to 0.001 and find that a smaller lr indeed improves the training stability under a large noise injection. Weight decay, as a popular regularization method in DNN training, can be used to avoid

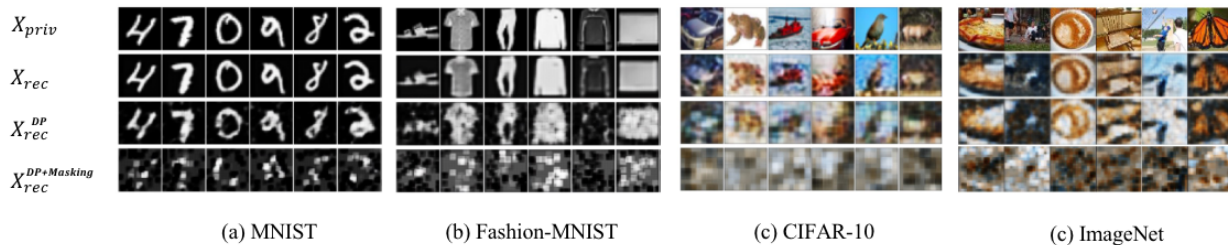


Figure 5: Private training data reconstruction by FSHA attack in Split Learning on MNIST and ImageNet. In all cases, X_{priv} : the original training data, i.e. ground truth; X_{rec} : FSHA on plain-text SplitNN; $X_{rec(N)}$: FSHA on SplitNN with noise injection (NI) ($\sigma = 0.7$); $X_{rec(S)}$: FSHA on SplitNN with NI and scaling ($\sigma = 0.7, \lambda = 0.2$); $X_{rec(M)}$: FSHA on SplitNN with NI and masking ($\sigma = 0.7, p = 0.2$). Models are split with one FC layer on the server side.

over-fitting on noisy signals. We find that only a heavy weight decay ($\gamma = 0.2, 0.4$) can help stabilize the training convergence till the end. However, a heavy weight decay sacrifices the convergence speed and fails to reach the baseline accuracy. Scaling can only improve the convergence at the beginning of the training, and none of them manage to maintain the convergence till the end. This implies an inherent training stability issue with noise injection, which cannot be alleviated by pure denoising. Therefore, we combine scaling with weight decay and find that a small weight decay ($\gamma = 0.01$) is sufficient to stabilize the training. On the contrary, the optimization of masking does not need weight decay. It can almost achieve the baseline convergence rate once the ratio p is properly tuned. Although there is a similarity between random masking and the dropout technique Srivastava et al. (2014), simply using dropout does not provide enough stability for the training, regardless of the dropout ratio. Both denoising techniques achieve significantly better training quality than standalone hyperparameter tuning. In §B.2, Table 5, we provide initial results of ResNet-18 on the CIFAR-100; our denoising techniques achieve higher accuracy than simple learning rate tuning. In Table 6 in §B.3, we demonstrate that the scaling postprocessing performs well even when Adam’s updating rule eliminates gradient scale impact. See limitations of the proposed approach in §C. In Table 7, we show the performance on the large-scale datasets. In addition, we discuss the different layers of the networks to split in §B.5 along with results in Table 8.

4.3 Attack defense

Setup. We demonstrate how the random masking technique can improve data privacy in defense against the recent feature-space hijacking attack (FSHA) Pasquini et al. (2021) in Split Learning. FSHA hijacks the client’s learning process from the server side during the training and performs the data reconstruction once the client’s output feature is learned; see details of threat model in §B.7. We evaluate the attack performance with 2 models and 4 publicly available datasets—CNN for MNIST and Fashion-MNIST, ResNet for CIFAR-10 and ImageNet. See the model configuration in Table 1. We compare the attack performance by visualizing the reconstructed private data between FSHA attacks on plain-text SplitNN, noise-injected SplitNN, and noise-injected SplitNN with masking or scaling. We focus on the case where only one FC layer is on the server because it is more resilient against data reconstruction attacks, see discussion in Figure 9 in §B.

Results. Figure 5 shows that the original FSHA can reconstruct the private data with very high accuracy for MNIST but only keeps the original images’ appearance for ImageNet. This is consistent with the attack performance in Pasquini et al. (2021)—attack on low-entropy images usually requires less effort and can produce a high-quality reconstruction. Next, we apply noise injection to the intermediate results and conduct data reconstruction on the perturbed data by FSHA. We observe that for MNIST, the digits on the reconstructed image are recognizable. For more complex and color image datasets (i.e. ImageNet), although noise can hide the details in the images, we can still relate the constructed image with the original one by looking at the outline or the background color. Lastly, when we combine noise injection with masking, the reconstructed images are fully damaged, and thus, the data security is greatly enhanced. While the scaling technique has almost no effect during the reconstruction attack, no matter how we set the scaling factor. See

Figures 10-12 in §B for results with different σ, p, λ and other datasets. Improving the privacy accounting for split learning is not the primary focus of this work, instead, we want to show how denoising can improve noisy SplitNN accuracy. Nevertheless, we provide the privacy bounds for one single forward pass during the SplitNN training in Table 11.

5 Conclusion

We propose scaling and masking as denoising techniques to achieve accurate Split Learning on noisy signals. We show theoretically and empirically that denoising helps achieve more accurate intermediate outputs in DNN training under noise injection that significantly improves the stability and accuracy of Split Learning. Additionally, we show that the masking technique can provide better security enhancement than scaling against powerful attacks. Although in theory, scaling has better denoising efficacy, masking is likely to show better accuracy improvement due to its easier parameter tuning. Finally, we demonstrate the possibility of co-optimization of denoising and attack defense.

References

- Martin Abadi, Andy Chu, Ian Goodfellow, H Brendan McMahan, Ilya Mironov, Kunal Talwar, and Li Zhang. Deep learning with differential privacy. In *Proceedings of the 2016 ACM SIGSAC conference on computer and communications security*, pp. 308–318, 2016.
- Sharif Abuadbba, Kyuyeon Kim, Minki Kim, Chandra Thapa, Seyit A. Camtepe, Yansong Gao, Hyounghick Kim, and Surya Nepal. Can we use split learning on 1d CNN models for privacy preserving training? In *Proceedings of the 15th ACM Asia Conference on Computer and Communications Security*, pp. 305–318, 2020.
- Borja Balle and Yu-Xiang Wang. Improving the gaussian mechanism for differential privacy: Analytical calibration and optimal denoising. In *International Conference on Machine Learning*, pp. 394–403. PMLR, 2018.
- El Houcine Bergou, Konstantin Burlachenko, Aritra Dutta, and Peter Richtárik. Personalized federated learning with communication compression. *Transactions on Machine Learning Research*, 2023.
- Garrett Bernstein, Ryan McKenna, Tao Sun, Daniel Sheldon, Michael Hay, and Gerome Miklau. Differentially private learning of undirected graphical models using collective graphical models. In *International Conference on Machine Learning*, pp. 478–487. PMLR, 2017.
- Alexander Camuto, Matthew Willetts, Umut Simsekli, Stephen J. Roberts, and Chris C. Holmes. Explicit regularisation in Gaussian noise injections. *Advances in Neural Information Processing Systems*, 33: 16603–16614, 2020.
- Alexander Camuto, Xiaoyu Wang, Lingjiong Zhu, Chris Holmes, Mert Gurbuzbalaban, and Umut Simsekli. Asymmetric heavy tails and implicit bias in gaussian noise injections. In *International Conference on Machine Learning*, pp. 1249–1260. PMLR, 2021.
- Tianyi Chen, Xiao Jin, Yuejiao Sun, and Wotao Yin. Vaf: A method of vertical asynchronous federated learning. *arXiv preprint arXiv:2007.06081*, 2020.
- Jia Deng, Wei Dong, Richard Socher, Li-Jia Li, Kai Li, and Li Fei-Fei. Imagenet: A large-scale hierarchical image database. In *IEEE Conference on Computer Vision and Pattern Recognition*, pp. 248–255, 2009.
- Cynthia Dwork, Guy N. Rothblum, and Salil Vadhan. Boosting and differential privacy. In *2010 IEEE 51st Annual Symposium on Foundations of Computer Science*, pp. 51–60, 2010.
- Cynthia Dwork, Aaron Roth, et al. The algorithmic foundations of differential privacy. *Found. Trends Theor. Comput. Sci.*, 9(3-4):211–407, 2014.

- Ege Erdogan, Alptekin Kupcu, and A Ercument Cicek. Unsplit: Data-oblivious model inversion, model stealing, and label inference attacks against split learning. *arXiv preprint arXiv:2108.09033*, 2021.
- Otkrist Gupta and Ramesh Raskar. Distributed learning of deep neural network over multiple agents. *Journal of Network and Computer Applications*, 116:1–8, 2018.
- Michael Hay, Chao Li, Gerome Miklau, and David Jensen. Accurate estimation of the degree distribution of private networks. In *2009 Ninth IEEE International Conference on Data Mining*, pp. 169–178. IEEE, 2009.
- Michael Hay, Vibhor Rastogi, Gerome Miklau, and Dan Suciu. Boosting the accuracy of differentially private histograms through consistency. *Proceedings of the VLDB Endowment*, 3(1), 2010.
- Zecheng He, Tianwei Zhang, and Ruby B Lee. Model inversion attacks against collaborative inference. In *Proceedings of the 35th Annual Computer Security Applications Conference*, pp. 148–162, 2019a.
- Zhezhi He, Adnan Siraj Rakin, and Deliang Fan. Parametric noise injection: Trainable randomness to improve deep neural network robustness against adversarial attack. In *Proceedings of the IEEE/CVF Conference on Computer Vision and Pattern Recognition*, pp. 588–597, 2019b.
- Sanjay Kariyappa and Moinuddin K Qureshi. Gradient inversion attack: Leaking private labels in two-party split learning. *arXiv preprint arXiv:2112.01299*, 2021.
- André I Khuri. *Advanced calculus with applications in statistics*. John Wiley & Sons, 2003.
- Alex Krizhevsky, Geoffrey Hinton, et al. Learning multiple layers of features from tiny images. 2009.
- Zhenzhong Lan, Mingda Chen, Sebastian Goodman, Kevin Gimpel, Piyush Sharma, and Radu Soricut. Albert: A lite bert for self-supervised learning of language representations. In *International Conference on Learning Representations*, 2020.
- Yann LeCun, Léon Bottou, Yoshua Bengio, and Patrick Haffner. Gradient-based learning applied to document recognition. *Proceedings of the IEEE*, 86(11):2278–2324, 1998.
- Mathias Lecuyer, Vaggelis Atlidakis, Roxana Geambasu, Daniel Hsu, and Suman Jana. Certified robustness to adversarial examples with differential privacy. In *2019 IEEE symposium on security and privacy (SP)*, pp. 656–672, 2019.
- Oscar Li, Jiankai Sun, Xin Yang, Weihao Gao, Hongyi Zhang, Junyuan Xie, Virginia Smith, and Chong Wang. Label leakage and protection in two-party split learning. *arXiv preprint arXiv:2102.08504*, 2021.
- Yinan Li and Fang Liu. Adaptive Gaussian Noise Injection Regularization for Neural Networks. In *International Symposium on Neural Networks*, pp. 176–189. Springer, 2020.
- Katrina Ligett, Seth Neel, Aaron Roth, Bo Waggoner, and Zhiwei Steven Wu. Accuracy first: Selecting a differential privacy level for accuracy-constrained ERM. *Advances in Neural Information Processing Systems*, 2017:2567–2577, 2017.
- Soon Hoe Lim, N. Benjamin Erichson, Liam Hodgkinson, and Michael W. Mahoney. Noisy recurrent neural networks. *Advances in Neural Information Processing Systems*, 34, 2021.
- Andrew Maas, Raymond E Daly, Peter T Pham, Dan Huang, Andrew Y Ng, and Christopher Potts. Learning word vectors for sentiment analysis. In *Proceedings of the 49th annual meeting of the association for computational linguistics: Human language technologies*, pp. 142–150, 2011.
- Julian McAuley and Jure Leskovec. Hidden Factors and Hidden Topics: Understanding Rating Dimensions with Review Text. In *ACM conference on Recommender systems*, pp. 165–172, 2013.
- Fatemehsadat Mireshghallah, Mohammadkazem Taram, Prakash Ramrakhiani, Ali Jalali, Dean Tullsen, and Hadi Esmaeilzadeh. Shredder: Learning noise distributions to protect inference privacy. In *Proceedings of the Twenty-Fifth International Conference on Architectural Support for Programming Languages and Operating Systems*, pp. 3–18, 2020.

- Milad Nasr and Reza Shokri. Improving deep learning with differential privacy using gradient encoding and denoising. *arXiv preprint arXiv:2007.11524*, 2020.
- Aleksandar Nikolov, Kunal Talwar, and Li Zhang. The geometry of differential privacy: the sparse and approximate cases. In *Proceedings of the forty-fifth annual ACM symposium on Theory of computing*, pp. 351–360, 2013.
- Dario Pasquini, Giuseppe Ateniese, and Massimo Bernaschi. Unleashing the tiger: Inference attacks on split learning. In *Proceedings of the 2021 ACM SIGSAC Conference on Computer and Communications Security*, pp. 2113–2129, 2021.
- Sean Robertson. NLP From Scratch: Classifying Names with a Character-Level RNN — PyTorch Tutorials, 2023. URL https://pytorch.org/tutorials/intermediate/char_rnn_classification_tutorial.html.
- Nitish Srivastava, Geoffrey Hinton, Alex Krizhevsky, Ilya Sutskever, and Ruslan Salakhutdinov. Dropout: a simple way to prevent neural networks from overfitting. *The journal of machine learning research*, 15(1): 1929–1958, 2014.
- Guangyu Sun, Matias Mendieta, Aritra Dutta, Xin Li, and Chen Chen. Towards multi-modal transformers in federated learning. In *European Conference on Computer Vision*, pp. 229–246. Springer, 2024.
- Yee Teh, David Newman, and Max Welling. A collapsed variational bayesian inference algorithm for latent dirichlet allocation. *Advances in neural information processing systems*, 19, 2006.
- Tom Titcombe, Adam J. Hall, Pavlos Papadopoulos, and Daniele Romanini. Practical defences against model inversion attacks for split neural networks. *arXiv preprint arXiv:2104.05743*, 2021.
- Praneeth Vepakomma, Otkrist Gupta, Tristan Swedish, and Ramesh Raskar. Split learning for health: Distributed deep learning without sharing raw patient data. *arXiv preprint arXiv:1812.00564*, 2018a.
- Praneeth Vepakomma, Tristan Swedish, Ramesh Raskar, Otkrist Gupta, and Abhimanyu Dubey. No peek: A survey of private distributed deep learning. *arXiv preprint arXiv:1812.03288*, 2018b.
- Praneeth Vepakomma, Otkrist Gupta, Abhimanyu Dubey, and Ramesh Raskar. Reducing leakage in distributed deep learning for sensitive health data. *arXiv preprint arXiv:1812.00564*, 2019.
- Bao Wang, Quanquan Gu, March Boedihardjo, Lingxiao Wang, Farzin Barekat, and Stanley J. Osher. DP-LSSGD: A stochastic optimization method to lift the utility in privacy-preserving ERM. In *Mathematical and Scientific Machine Learning*, pp. 328–351. PMLR, 2020a.
- Chang Wang, Jian Liang, Mingkai Huang, Bing Bai, Kun Bai, and Hao Li. Hybrid differentially private federated learning on vertically partitioned data. *arXiv preprint arXiv:2009.02763*, 2020b.
- Ji Wang, Jianguo Zhang, Weidong Bao, Xiaomin Zhu, Bokai Cao, and Philip S. Yu. Not just privacy: Improving performance of private deep learning in mobile cloud. In *Proceedings of the 24th ACM SIGKDD international conference on knowledge discovery & data mining*, pp. 2407–2416, 2018.
- Wenxiao Wang, Tianhao Wang, Lun Wang, Nanqing Luo, Pan Zhou, Dawn Song, and Ruoxi Jia. Dplis: Boosting utility of differentially private deep learning via randomized smoothing. *Proceedings on Privacy Enhancing Technologies*, 4:163–183, 2021.
- Maoqiang Wu, Guoliang Cheng, Peichun Li, Rong Yu, Yuan Wu, Miao Pan, and Rongxing Lu. Split learning with differential privacy for integrated terrestrial and non-terrestrial networks. *IEEE Wireless Communications*, pp. 1–8, 2023. doi: 10.1109/MWC.015.2200462.
- Liyao Xiang, Jingbo Yang, and Baochun Li. Differentially-private deep learning from an optimization perspective. In *IEEE INFOCOM 2019 - IEEE Conference on Computer Communications*, pp. 559–567, 2019.

Hang Xu, Kelly Kostopoulou, Aritra Dutta, Xin Li, Alexandros Ntoulas, and Panos Kalnis. Deepreduce: A sparse-tensor communication framework for federated deep learning. *Advances in Neural Information Processing Systems*, 34:21150–21163, 2021.

Ashkan Yousefpour, Igor Shilov, Alexandre Sablayrolles, Davide Testuggine, Karthik Prasad, Mani Malek, John Nguyen, Sayan Ghosh, Akash Bharadwaj, Jessica Zhao, et al. Opacus: User-friendly differential privacy library in pytorch. *arXiv preprint arXiv:2109.12298*, 2021.

Yuheng Zhang, Ruoxi Jia, Hengzhi Pei, Wenxiao Wang, Bo Li, and Dawn Song. The secret revealer: Generative model-inversion attacks against deep neural networks. In *Proceedings of the IEEE/CVF Conference on Computer Vision and Pattern Recognition*, pp. 253–261, 2020.

Keyu Zhu, Pascal Van Hentenryck, and Ferdinando Fioretto. Bias and variance of post-processing in differential privacy. In *Proceedings of the AAAI Conference on Artificial Intelligence*, volume 35, pp. 11177–11184, 2021.

Keyu Zhu, Ferdinando Fioretto, and Pascal Van Hentenryck. Post-processing of differentially private data: A fairness perspective. In *International Joint Conference on Artificial Intelligence (IJCAI)*, 2022.

Contents

1	Introduction	1
2	Related Work	2
3	Theoretical Guarantee	3
3.1	A linear layer	4
3.2	Nonlinear loss function for classification task	5
3.3	Differential privacy (DP) preservation	6
4	Experimental Evaluation	7
4.1	Simulation	8
4.2	DNN Experiments	8
4.3	Attack defense	10
5	Conclusion	11
A	Theoretical guarantee	16
A.1	Definitions	16
A.2	ℓ_2 Regression task	16
A.3	Nonlinear loss function for classification task	18
A.3.1	Proof of Theorem 3.4	20
A.3.2	Sketch of Proof of Theorem 3.5	22
A.3.3	Concentration of the errors	23
A.4	Differential Privacy (DP)	23
A.4.1	DP of the gradient during backpropagation	24
B	Addendum to the Numerical Results	25
B.1	Laplace mechanism	26
B.2	Split learning result on CIFAR-100	26
B.3	Understanding the scaling operation when gradient scale impact is eliminated	26
B.4	Split learning on large datasets	28
B.5	Experiments on Split Position	28
B.6	Computational overhead of the postprocessing functions	28
B.7	Feature-space hijacking attack (FSHA) and our post-processing techniques	30
B.8	DP budget	34
C	Limitations	34

A Theoretical guarantee

First, we will start with the definition of softmax and negative log loss functions used for nonlinear classification.

A.1 Definitions

Softmax and negative log loss. Let m be the number of classes. For a vector, $z \in \mathbb{R}^m$, the softmax function, $s : \mathbb{R}^m \rightarrow (0, 1)^m$, is defined as

$$s(z)_i = \frac{e^{z_i}}{\sum_{i=1}^m e^{z_i}}.$$

Let y be a binary indicator (0 or 1) of the class label, and c is the correct classification of the observation, o . Denote $p_{o,c}$ as the predicted probability of observation o that belongs to class c . Then the negative log-loss function is defined as

$$\mathcal{L}_{LL}(y, p) = - \sum_{c=1}^m y_{o,c} \log(p_{o,c}).$$

What loss functions and tasks do we cover? In general, for classification problems such as image classification by CNN, movie review prediction by RNN, and many more, the output layer is configured with a softmax function for prediction, and the negative log function is used as the loss function to train the DNN model. For binary classification, this loss is known as binary cross-entropy; for multi-class classification, it is called categorical cross-entropy. MSE is a consequence of Theorem 3.1 with some modifications. Therefore, our analyses cover almost all the existing loss functions used for DNN training. We refrain from using some rarely used loss functions, e.g., sparse categorical cross-entropy.

A.2 ℓ_2 Regression task

Proof of Theorem 3.1.

Proof. (i) We are required to show, $\mathbb{E}\|MX - M\tilde{X}\|_2^2 - \mathbb{E}\|MX - MR_p(\tilde{X})\|_2^2 \geq 0$. There are two types of randomness involved—one is due to randomness in R_p , and the second is due to the randomness in \tilde{X} . First, we start by writing

$$\begin{aligned} & \|MX - M\tilde{X}\|_2^2 \\ &= \|MX\|_2^2 - 2\langle MX, M\tilde{X} \rangle + \sum_{i=1}^m \sum_{j=1}^n m_{ij}^2 \tilde{x}_j^2 + 2 \sum_{i=1}^m \sum_{1 \leq j < k \leq n} m_{ij} m_{ik} \tilde{x}_j \tilde{x}_k, \end{aligned} \quad (5)$$

which after taking expectation becomes

$$\begin{aligned} & E[\|MX - M\tilde{X}\|_2^2] \\ &= -\|MX\|_2^2 + \sum_{i=1}^m \sum_{j=1}^n m_{ij}^2 (x_j^2 + \sigma^2) + 2 \sum_{i=1}^m \sum_{1 \leq j < k \leq n} m_{ij} m_{ik} x_j x_k. \end{aligned} \quad (6)$$

Next, we have as in (5)

$$\begin{aligned} & \|MX - MR_p(\tilde{X})\|_2^2 \\ &= \|MX\|_2^2 - 2\langle MX, MR_p(\tilde{X}) \rangle + \sum_{i=1}^m \sum_{j=1}^n m_{ij}^2 (R_p(\tilde{x}_j))^2 + 2 \sum_{i=1}^m \sum_{1 \leq j < k \leq n} m_{ij} m_{ik} R_p(\tilde{x}_j) R_p(\tilde{x}_k), \end{aligned} \quad (7)$$

which after taking expectation conditioned on the randomness in R_p given \tilde{X} becomes

$$\begin{aligned} & E_p[\|MX - MR_p(\tilde{X})\|_2^2 | \tilde{X}] \\ &= \|MX\|_2^2 - 2p\langle MX, M\tilde{X} \rangle + p \sum_{i=1}^m \sum_{j=1}^n m_{ij}^2 \tilde{x}_j^2 + 2p^2 \sum_{i=1}^m \sum_{1 \leq j < k \leq n} m_{ij} m_{ik} \tilde{x}_j \tilde{x}_k. \end{aligned} \quad (8)$$

Finally, taking the expectation on the randomness in \tilde{X} we obtain

$$\begin{aligned} & \mathbb{E}_Z E_p[\|MX - MR_p(\tilde{X})\|_2^2 | \tilde{X}] \\ &= (1 - 2p)\|MX\|_2^2 + p \sum_{i=1}^m \sum_{j=1}^n m_{ij}^2 (x_j^2 + \sigma^2) + 2p^2 \sum_{i=1}^m \sum_{1 \leq j < k \leq n} m_{ij} m_{ik} x_j x_k. \end{aligned} \quad (9)$$

In view of equation 6 and equation 9, we have

$$\begin{aligned} & E[\|MX - M\tilde{X}\|_2^2] - E[\|MX - MR_p(\tilde{X})\|_2^2] \\ &= (2p - 2)\|MX\|_2^2 + (1 - p) \sum_{i=1}^m \sum_{j=1}^n m_{ij}^2 (x_j^2 + \sigma^2) + 2(1 - p^2) \sum_{i=1}^m \sum_{1 \leq j < k \leq n} m_{ij} m_{ik} x_j x_k \\ &= (2p - 2) \left[\sum_{i=1}^m \sum_{j=1}^n m_{ij}^2 x_j^2 + 2 \sum_{i=1}^m \sum_{1 \leq j < k \leq n} m_{ij} m_{ik} x_j x_k \right] + (1 - p) \sum_{i=1}^m \sum_{j=1}^n m_{ij}^2 (x_j^2 + \sigma^2) \\ &\quad + 2(1 - p^2) \sum_{i=1}^m \sum_{1 \leq j < k \leq n} m_{ij} m_{ik} x_j x_k \\ &= (1 - p) \sum_{i=1}^m \sum_{j=1}^n m_{ij}^2 (\sigma^2 - x_j^2) - 2(1 - p)^2 \sum_{i=1}^m \sum_{1 \leq j < k \leq n} m_{ij} m_{ik} x_j x_k. \end{aligned} \quad (10)$$

Therefore,

$$\mathbb{E}\|MX - M\tilde{X}\|_2^2 - \mathbb{E}\|MX - MR_p(\tilde{X})\|_2^2 \geq 0$$

if and only if the expression in equation 10 is non-negative, that is,

$$\sum_{i=1}^m \sum_{j=1}^n m_{ij}^2 \sigma^2 \geq \sum_{i=1}^m \sum_{j=1}^n m_{ij}^2 x_j^2 + 2(1 - p) \sum_{i=1}^m \sum_{1 \leq j < k \leq n} m_{ij} m_{ik} x_j x_k.$$

The left hand side of the above expression is $\sigma^2 \|M\|_F^2$ (which is lower bounded by $n\sigma^2 \sigma_{\min}^2(M)$, where $\sigma_{\min}(M)$ is the smallest singular value of M). For the right-hand side, we have

$$\begin{aligned} & \sum_{i=1}^m \sum_{j=1}^n m_{ij}^2 x_j^2 + 2(1 - p) \sum_{i=1}^m \sum_{1 \leq j < k \leq n} m_{ij} m_{ik} x_j x_k \\ &= p \sum_{i=1}^m \sum_{j=1}^n m_{ij}^2 x_j^2 + (1 - p) \sum_{i=1}^m \sum_{j=1}^n m_{ij}^2 x_j^2 + 2(1 - p) \sum_{i=1}^m \sum_{1 \leq j < k \leq n} m_{ij} m_{ik} x_j x_k \\ &= p \sum_{i=1}^m \sum_{j=1}^n m_{ij}^2 x_j^2 + (1 - p)\|MX\|_2^2 \\ &= p\|M \odot \bar{X}\|_F^2 + (1 - p)\|MX\|_2^2, \end{aligned} \quad (11)$$

where $\bar{X} = \begin{pmatrix} x_1 & x_2 & x_3 & \cdots & x_n \\ x_1 & x_2 & x_3 & \cdots & x_n \\ \cdots & \cdots & \cdots & \cdots & \cdots \\ x_1 & x_2 & x_3 & \cdots & x_n \end{pmatrix} \in \mathbb{R}^{m \times n}$. Therefore,

$$\mathbb{E}\|MX - M\tilde{X}\|_2^2 - \mathbb{E}\|MX - MR_p(\tilde{X})\|_2^2 \geq 0$$

if and only if

$$\sigma^2 \|M\|_F^2 \geq p\|M \odot \bar{X}\|_F^2 + (1 - p)\|MX\|_2^2.$$

Hence the result.

(ii) We are required to show, $\mathbb{E}\|MX - M\tilde{X}\|_2^2 - \mathbb{E}\|MX - MS_\alpha(\tilde{X})\|_2^2 \geq 0$. Note that, the only randomness involved in this case is due to the randomness in \tilde{X} . First, we start by expanding

$$\begin{aligned} & \|MX - MS_\alpha(\tilde{X})\|_2^2 \\ &= \|MX\|_2^2 - \frac{2}{\alpha} \langle MX, M\tilde{X} \rangle + \sum_{i=1}^m \sum_{j=1}^n m_{ij}^2 \frac{\tilde{x}_j^2}{\alpha^2} + 2 \sum_{i=1}^m \sum_{1 \leq j < k \leq n} m_{ij} m_{ik} \frac{\tilde{x}_j \tilde{x}_k}{\alpha^2}, \end{aligned} \quad (12)$$

which after taking expectation gives

$$\begin{aligned} & E[\|MX - MS_\alpha(\tilde{X})\|_2^2] \\ &= \left(1 - \frac{2}{\alpha}\right) \|MX\|_2^2 + \sum_{i=1}^m \sum_{j=1}^n m_{ij}^2 \frac{(x_j^2 + \sigma^2)}{\alpha^2} + 2 \sum_{i=1}^m \sum_{1 \leq j < k \leq n} m_{ij} m_{ik} \frac{x_j x_k}{\alpha^2} \\ &= \left(1 - \frac{1}{\alpha}\right)^2 \|MX\|_2^2 + \frac{\sigma^2}{\alpha^2} \|M\|_F^2. \end{aligned} \quad (13)$$

In view of equation 6 and equation 13, we have

$$\begin{aligned} & E[\|MX - M\tilde{X}\|_2^2] - E[\|MX - MS_\alpha(\tilde{X})\|_2^2] \\ &= \left(1 - \frac{1}{\alpha^2}\right) \sigma^2 \|M\|_F^2 - \left(1 - \frac{1}{\alpha}\right)^2 \|MX\|_2^2. \end{aligned}$$

Therefore,

$$\mathbb{E}\|MX - M\tilde{X}\|_2^2 - \mathbb{E}\|MX - MS_\alpha(\tilde{X})\|_2^2 \geq 0$$

if and only if $(1 + \frac{1}{\alpha})\sigma^2 \|M\|_F^2 - (1 - \frac{1}{\alpha})\|MX\|_2^2 \geq 0$. This completes our proof. \square

A.3 Nonlinear loss function for classification task

Now, we will prove the results for the nonlinear loss function as given in Section 3.2. First, we quote the following Lemma about the moment generating function of a random variable, without proof. The readers can find the proof of Lemma A.1 in any standard graduate statistics textbook.

Lemma A.1. *Let Z be a random variable, $Z \sim N(\mu, \sigma^2)$. Then the moment generating function, $\Phi_Z(\cdot)$ is given by $\Phi_Z(t) = \mathbb{E}e^{tZ} = e^{\mu t + \frac{\sigma^2 t^2}{2}}$.*

Calculating $\mathbb{E}\mathcal{L}_{LL}(y^*, s(MR_p(\tilde{X})))$ requires some auxiliary results on the $\mathbb{E}\sum_{i=1}^m e^{(MR_p(\tilde{X}))_i}$ and $\mathbb{E}\left(\sum_{i=1}^m e^{(MR_p(\tilde{X}))_i}\right)^2$. The following Lemma A.2 gives the details, which are necessary for calculating the expectation and the variance of $\sum_{i=1}^m e^{(MR_p(\tilde{X}))_i}$.

Lemma A.2. *We have, (i) $\mathbb{E}\sum_{i=1}^m e^{(MR_p(\tilde{X}))_i} = \sum_{i=1}^m \prod_{k=1}^n \left(p e^{m_{ik} x_k + \frac{m_{ik}^2 \sigma^2}{2}} + (1-p) \right)$; and (ii) $\mathbb{E}\left(\sum_{i=1}^m e^{(MR_p(\tilde{X}))_i}\right)^2 = \sum_{i,j} \left[\prod_{k=1}^n \left(p e^{(m_{ik} + m_{jk}) x_k + \frac{(m_{ik} + m_{jk})^2 \sigma^2}{2}} + (1-p) \right) \right]$.*

Proof. (i) We have

$$\sum_{i=1}^m e^{(MR_p(\tilde{X}))_i} = \sum_{i=1}^m e^{\sum_{k=1}^n m_{ik} R_p(\tilde{x}_k)}, \quad (14)$$

where \tilde{x}_k be the k^{th} element of the vector \tilde{X} . Note that, each $m_{ik} R_p(\tilde{x}_k)$ is independent (based on the definition of the random masking operator), and after taking expectation on the above expression with respect to the randomness in R_p , we have

$$\mathbb{E}_p \sum_{i=1}^m e^{(MR_p(\tilde{X}))_i} = \sum_{i=1}^m \prod_{k=1}^n \mathbb{E}_p e^{m_{ik} R_p(\tilde{x}_k)}. \quad (15)$$

For $p \in (0, 1]$, equation 15 becomes

$$\mathbb{E}_p \sum_{i=1}^m e^{(MR_p(\tilde{X}))_i} = \sum_{i=1}^m \prod_{k=1}^n \mathbb{E}_p e^{m_{ik} R_p(\tilde{x}_k)} = \sum_{i=1}^m \prod_{k=1}^n (pe^{m_{ik} \tilde{x}_k} + (1-p)e^{m_{ik} \cdot 0}), \quad (16)$$

which further taking expectation on the randomness in \tilde{X} reduces to

$$\begin{aligned} \mathbb{E}_Z \mathbb{E}_p \sum_{i=1}^m e^{(MR_p(\tilde{X}))_i} &= \sum_{i=1}^m \prod_{k=1}^n (\mathbb{E}_Z p e^{m_{ik} \tilde{x}_k} + (1-p)) \\ &\stackrel{\text{Lemma A.1}}{=} \sum_{i=1}^m \prod_{k=1}^n \left(p e^{m_{ik} x_k + \frac{m_{ik}^2 \sigma^2}{2}} + (1-p) \right). \end{aligned} \quad (17)$$

After taking total expectation on equation 17 and by using the tower property of expectation, we obtain the result.

(ii) We have

$$\left(\sum_{i=1}^m e^{(MR_p(\tilde{X}))_i} \right)^2 = \sum_{i,j} e^{\sum_{k=1}^n (m_{ik} + m_{jk}) R_p(\tilde{x}_k)}. \quad (18)$$

Proceeding similarly as above, first, taking expectation on the above expression with respect to the randomness in R_p and then taking expectation with respect to the randomness in \tilde{X} , we have

$$\begin{aligned} \mathbb{E}_Z \mathbb{E}_p \left(\sum_{i=1}^m e^{(MR_p(\tilde{X}))_i} \right)^2 &= \mathbb{E}_Z \mathbb{E}_p \sum_{i,j} \left(e^{\sum_{k=1}^n (m_{ik} + m_{jk}) R_p(\tilde{x}_k)} \right) \\ &= \mathbb{E}_Z \sum_{i,j} \prod_{k=1}^n \mathbb{E}_p e^{(m_{ik} + m_{jk}) R_p(\tilde{x}_k)} \\ &= \mathbb{E}_Z \sum_{i,j} \prod_{k=1}^n \left(p e^{(m_{ik} + m_{jk}) \tilde{x}_k} + (1-p) \right) \\ &\stackrel{\text{Lemma A.1}}{=} \sum_{i,j} \prod_{k=1}^n \left(p e^{(m_{ik} + m_{jk}) x_k + \frac{(m_{ik} + m_{jk})^2 \sigma^2}{2}} + (1-p) \right). \end{aligned} \quad (19)$$

After taking total expectation on equation 19 and by using the tower property of expectation, we obtain the result. \square

Remark A.3. Setting $p = 1$, in the loss function, we find the expected loss value, $\mathbb{E} \mathcal{L}_{LL}(y^*, s(M\tilde{X}))$ due to noise injection (without random masking). Additionally, for $p = 1$, in Lemma A.2, we recover $\mathbb{E} \sum_{i=1}^m e^{(M\tilde{X})_i} = \sum_{i=1}^m \prod_{k=1}^n (e^{m_{ik} x_k + \frac{m_{ik}^2 \sigma^2}{2}})$.

The following Lemma¹, is the next intermediate result and instrumental in proving our main result as it approximates the expected logarithmic term in the log loss. In Lemma A.4, we approximate $\mathbb{E}[\log(x)]$ by using Taylor's Theorem.

Lemma A.4. (*Khuri, 2003, p. 117*) *Let x be a positive random variable. Then $\mathbb{E}[\log(x)] = \log[\mathbb{E}(x)] - \frac{\text{Var}(x)}{2(\mathbb{E}(x))^2} + \text{higher order terms}$, where $\text{Var}(x) = \mathbb{E}(x^2) - (\mathbb{E}(x))^2$.*

Remark A.5. We assume that x have small higher order moments, $m_p = \mathbb{E}|x - \mathbb{E}(x)|^p$, for $p = 2, 3, \dots$.

Note that, setting $x = \sum_{i=1}^m e^{(MR_p(\tilde{X}))_i}$ in Lemma A.4 is the first step to quantify the expected loss value of SplitNN with random masking, $\mathbb{E} \mathcal{L}_{LL}(y^*, s(MR_p(\tilde{X})))$.

¹See similar expression in Teh et al. (2006) with a restrictive assumption; assumption in Lemma A.4 is more general.

A.3.1 Proof of Theorem 3.4

To prove Theorem 3.4, recall that $\mathcal{F}(p) := \mathbb{E}\mathcal{L}_{LL}(y^*, s(MR_p(\tilde{X})))$, and consequently, $\mathcal{F}(1) = \mathbb{E}\mathcal{L}_{LL}(y^*, s(M\tilde{X}))$. By using Lemma A.4 and assuming the higher order terms are negligible, we write

$$\mathcal{F}(p) = \underbrace{-p(MX)_{i^*}}_{:=\mathcal{B}(p)} + \underbrace{\log\left(\mathbb{E}\sum_{i=1}^m e^{(MR_p(\tilde{X}))_i}\right)}_{:=\mathcal{C}(p)} - \underbrace{\frac{\text{Var}\left(\sum_{i=1}^m e^{(MR_p(\tilde{X}))_i}\right)}{2\left(\mathbb{E}\sum_{i=1}^m e^{(MR_p(\tilde{X}))_i}\right)^2}}_{:=\mathcal{D}(p)}. \quad (20)$$

Differentiating equation 20 with respect to p gives us:

$$\mathcal{F}'(p) = \mathcal{B}'(p) + \mathcal{C}'(p) - \mathcal{D}'(p).$$

Note that,

$$\mathcal{B}'(p) = -(MX)_{i^*}, \mathcal{C}'(p) = \frac{\frac{d}{dp}\left(\mathbb{E}\sum_{i=1}^m e^{(MR_p(\tilde{X}))_i}\right)}{\mathbb{E}\sum_{i=1}^m e^{(MR_p(\tilde{X}))_i}},$$

but the derivative of $\mathcal{D}(p)$ becomes very messy. So, we take the following indirect route: we first show that (i) $\mathcal{B}'(1) + \mathcal{C}'(1) \geq 0$ and hence $\mathcal{B}(p) + \mathcal{C}(p)$ are increasing in a neighborhood to the left of $p = 1$; then we verify that (ii) $-\mathcal{D}'(p) \leq -\mathcal{D}'(1)$. We see that once we accomplish (i) and (ii), we will have $\mathcal{F}(p) \leq \mathcal{F}(1)$, which completes the proof of Theorem 3.4.

Proof of (i).

By Lemme A.2 and a straightforward computation, we have

$$\left.\frac{d}{dp}\left(\mathbb{E}\sum_{i=1}^m e^{(MR_p(\tilde{X}))_i}\right)\right|_{p=1} = \sum_{i=1}^m \sum_{r=1}^n \left[\left(e^{m_{ir}x_r + \frac{m_{ir}^2\sigma^2}{2}} - 1 \right) \prod_{k \neq r, k=1}^n e^{m_{ik}x_k + \frac{m_{ik}^2\sigma^2}{2}} \right].$$

So,

$$\mathcal{B}'(1) + \mathcal{C}'(1) = -(MX)_i + \frac{\sum_{i=1}^m \sum_{r=1}^n \left[\left(e^{m_{ir}x_r + \frac{m_{ir}^2\sigma^2}{2}} - 1 \right) \prod_{k \neq r, k=1}^n \left(e^{m_{ik}x_k + \frac{m_{ik}^2\sigma^2}{2}} \right) \right]}{\sum_{i=1}^m \left(\prod_{k=1}^n \left(e^{m_{ik}x_k + \frac{m_{ik}^2\sigma^2}{2}} \right) \right)},$$

which is bigger than or equal to 0 if and only if

$$\frac{\sum_{i=1}^m \sum_{r=1}^n \left[\left(e^{m_{ir}x_r + \frac{m_{ir}^2\sigma^2}{2}} - 1 \right) \prod_{k \neq r, k=1}^n \left(e^{m_{ik}x_k + \frac{m_{ik}^2\sigma^2}{2}} \right) \right]}{\sum_{i=1}^m \left(\prod_{k=1}^n \left(e^{m_{ik}x_k + \frac{m_{ik}^2\sigma^2}{2}} \right) \right)} \geq (MX)_{i^*}, \quad (21)$$

or equivalently,

$$\sum_{i=1}^m \sum_{r=1}^n \left[\left(e^{m_{ir}x_r + \frac{m_{ir}^2\sigma^2}{2}} - 1 \right) \prod_{k \neq r, k=1}^n \left(e^{m_{ik}x_k + \frac{m_{ik}^2\sigma^2}{2}} \right) \right] \geq (MX)_{i^*} \sum_{i=1}^m \left(\prod_{k=1}^n \left(e^{m_{ik}x_k + \frac{m_{ik}^2\sigma^2}{2}} \right) \right).$$

Let $f(\sigma^2)$ denote the difference of the two sides, we have $f(\sigma^2) :=$

$$\begin{aligned} & \sum_{i=1}^m \left[\sum_{r=1}^n \left(e^{m_{i^*r}x_r + \frac{m_{i^*r}^2\sigma^2}{2}} - 1 \right) \prod_{k \neq r, k=1}^n \left(e^{m_{ik}x_k + \frac{m_{ik}^2\sigma^2}{2}} \right) \right] - (MX)_{i^*} \sum_{i=1}^m \prod_{k=1}^n \left(e^{m_{ik}x_k + \frac{m_{ik}^2\sigma^2}{2}} \right) \\ &= \sum_{i=1}^m \left(\prod_{k=1}^n e^{m_{ik}x_k + \frac{m_{ik}^2\sigma^2}{2}} \right) \left[-(MX)_{i^*} + \sum_{r=1}^n \left(1 - e^{-m_{i^*r}x_r - \frac{m_{i^*r}^2\sigma^2}{2}} \right) \right] \\ &= \sum_{i=1}^m \left(\prod_{k=1}^n e^{m_{ik}x_k + \frac{m_{ik}^2\sigma^2}{2}} \right) \left[\sum_{r=1}^n \left(1 - m_{i^*r}x_r - e^{-m_{i^*r}x_r - \frac{m_{i^*r}^2\sigma^2}{2}} \right) \right]. \end{aligned}$$

Now, note that $\sum_{r=1}^n (1 - m_{i^*r}x_r - e^{-m_{i^*r}x_r - \frac{m_{i^*r}^2\sigma^2}{2}})$ is an increasing function of σ^2 and as $\sigma^2 \rightarrow +\infty$, it approaches $\sum_{r=1}^n (1 - m_{i^*r}x_r) = n - \sum_{r=1}^n m_{i^*r}x_r$, which is positive by assumption. Thus, when σ^2 is large enough, $f(\sigma^2) > 0$. This verifies (21) and hence (i).

Proof of (ii).

We need to verify that $\mathcal{D}(p) \geq \mathcal{D}(1)$, that is, by the definition of $\mathcal{D}(p)$,

$$\frac{\text{Var} \left(\sum_{i=1}^m e^{(MR_p(\tilde{X}))_i} \right)}{2 \left(\mathbb{E} \sum_{i=1}^m e^{(MR_p(\tilde{X}))_i} \right)^2} \geq \frac{\text{Var} \left(\sum_{i=1}^m e^{(MR_p(\tilde{X}))_i} \right)}{2 \left(\mathbb{E} \sum_{i=1}^m e^{(MR_p(\tilde{X}))_i} \right)^2} \Bigg|_{p=1}.$$

By the formula $\text{Var}(x) = \mathbb{E}x^2 - (\mathbb{E}x)^2$, it suffices to verify

$$\begin{aligned} & \frac{\mathbb{E} \left(\sum_{i=1}^m e^{(MR_p(\tilde{X}))_i} \right)^2 - \left(\mathbb{E} \sum_{i=1}^m e^{(MR_p(\tilde{X}))_i} \right)^2}{2 \left(\mathbb{E} \left(\sum_{i=1}^m e^{(MR_p(\tilde{X}))_i} \right) \right)^2} \\ & \geq \frac{\mathbb{E} \left(\sum_{i=1}^m e^{(MR_p(\tilde{X}))_i} \right)^2 - \left(\mathbb{E} \sum_{i=1}^m e^{(MR_p(\tilde{X}))_i} \right)^2}{2 \left(\mathbb{E} \left(\sum_{i=1}^m e^{(MR_p(\tilde{X}))_i} \right) \right)^2} \Bigg|_{p=1}. \end{aligned}$$

which can be simplified to

$$\frac{\mathbb{E} \left(\sum_{i=1}^m e^{(MR_p(\tilde{X}))_i} \right)^2}{\left(\mathbb{E} \left(\sum_{i=1}^m e^{(MR_p(\tilde{X}))_i} \right) \right)^2} \geq \frac{\mathbb{E} \left(\sum_{i=1}^m e^{(MR_p(\tilde{X}))_i} \right)^2}{\left(\mathbb{E} \left(\sum_{i=1}^m e^{(MR_p(\tilde{X}))_i} \right) \right)^2} \Bigg|_{p=1}.$$

Using Lemma A.2, the above is the same as

$$\frac{\sum_{i,j}^m \prod_{k=1}^n \left[p e^{(m_{ik}+m_{jk})x_k + \frac{(m_{ik}+m_{jk})^2\sigma^2}{2}} + (1-p) \right]}{\left[\sum_{i=1}^m \prod_{k=1}^n \left(p e^{m_{ik}x_k + \frac{m_{ik}^2\sigma^2}{2}} + (1-p) \right) \right]^2} \geq \frac{\sum_{i,j}^m \prod_{k=1}^n e^{(m_{ik}+m_{jk})x_k + \frac{(m_{ik}+m_{jk})^2\sigma^2}{2}}}{\left(\sum_{i=1}^m \prod_{k=1}^n e^{m_{ik}x_k + \frac{m_{ik}^2\sigma^2}{2}} \right)^2}. \quad (22)$$

We now verify (22) for σ^2 large enough. Note that (22) is true if and only if the following function $g(p) \geq 0$ where

$$\begin{aligned} g(p) &:= \sum_{i,j}^m \prod_{k=1}^n \left[p e^{(m_{ik}+m_{jk})x_k + \frac{(m_{ik}+m_{jk})^2\sigma^2}{2}} + (1-p) \right] \left(\sum_{i=1}^m \prod_{k=1}^n e^{m_{ik}x_k + \frac{m_{ik}^2\sigma^2}{2}} \right)^2 \\ &\quad - \sum_{i,j}^m \prod_{k=1}^n \left(e^{(m_{ik}+m_{jk})x_k + \frac{(m_{ik}+m_{jk})^2\sigma^2}{2}} \right) \left[\sum_{i=1}^m \prod_{k=1}^n \left(p e^{m_{ik}x_k + \frac{m_{ik}^2\sigma^2}{2}} + (1-p) \right) \right]^2. \end{aligned}$$

Note that $g(1) = 0$. So, it suffices to show that $g(p)$ is non-increasing on a small neighborhood to the left-hand side of 1. Differentiate g to get

$$g'(1) = \sum_{i,j}^m \prod_{k=1}^n \left(e^{(m_{ik}+m_{jk})x_k + \frac{(m_{ik}+m_{jk})^2\sigma^2}{2}} \right) \sum_{r=1}^n \left(1 - e^{-(m_{ir}+m_{jr})x_r - \frac{(m_{ir}+m_{jr})^2\sigma^2}{2}} \right) \times I^2 \\ - J \times 2I \times \sum_{i=1}^m \prod_{k=1}^n \left(e^{m_{ik}x_k + \frac{m_{ik}^2\sigma^2}{2}} \right) \sum_{r=1}^n \left(1 - e^{-m_{ir}x_r - \frac{m_{ir}^2\sigma^2}{2}} \right).$$

where $I := \sum_{i=1}^m \prod_{k=1}^n e^{m_{ik}x_k + \frac{m_{ik}^2\sigma^2}{2}}$ and $J := \sum_{i,j}^m \prod_{k=1}^n e^{(m_{ik}+m_{jk})x_k + \frac{(m_{ik}+m_{jk})^2\sigma^2}{2}}$. We have

$$g'(1) = I \left\{ \sum_{i,j}^m \prod_{k=1}^n \left(e^{(m_{ik}+m_{jk})x_k + \frac{(m_{ik}+m_{jk})^2\sigma^2}{2}} \right) \sum_{r=1}^n \left(1 - e^{-(m_{ir}+m_{jr})x_r - \frac{(m_{ir}+m_{jr})^2\sigma^2}{2}} \right) \times I \right. \\ \left. - J \times 2 \times \sum_{i=1}^m \prod_{k=1}^n e^{m_{ik}x_k + \frac{m_{ik}^2\sigma^2}{2}} \sum_{r=1}^n \left(1 - e^{-m_{ir}x_r - \frac{m_{ir}^2\sigma^2}{2}} \right) \right\} \\ = I \left\{ \sum_{i,j}^m \prod_{k=1}^n e^{(m_{ik}+m_{jk})x_k + \frac{(m_{ik}+m_{jk})^2\sigma^2}{2}} \left(n - \sum_{r=1}^n e^{-(m_{ir}+m_{jr})x_r - \frac{(m_{ir}+m_{jr})^2\sigma^2}{2}} \right) \times I \right. \\ \left. - J \times 2 \times \sum_{i=1}^m \prod_{k=1}^n e^{m_{ik}x_k + \frac{m_{ik}^2\sigma^2}{2}} \left(n - \sum_{r=1}^n e^{-m_{ir}x_r - \frac{m_{ir}^2\sigma^2}{2}} \right) \right\} \\ = I \left\{ n \times I \times J - \sum_{i,j,s}^m \prod_{k=1}^n e^{(m_{ik}+m_{jk}+m_{sk})x_k + \frac{((m_{ik}+m_{jk})^2+m_{sk}^2)\sigma^2}{2}} \sum_{r=1}^n e^{-(m_{ir}+m_{jr})x_r - \frac{(m_{ir}+m_{jr})^2\sigma^2}{2}} \right. \\ \left. - 2n \times J \times I + 2 \sum_{i,j,s=1}^m \prod_{k=1}^n e^{(m_{ik}+m_{jk}+m_{sk})x_k + \frac{((m_{ik}+m_{jk})^2+m_{sk}^2)\sigma^2}{2}} \sum_{r=1}^n e^{-m_{sr}x_r - \frac{m_{sr}^2\sigma^2}{2}} \right\} \\ = I \left\{ -n \times I \times J - \sum_{i,j,s}^m \prod_{k=1}^n e^{(m_{ik}+m_{jk}+m_{sk})x_k + \frac{((m_{ik}+m_{jk})^2+m_{sk}^2)\sigma^2}{2}} \sum_{r=1}^n e^{-(m_{ir}+m_{jr})x_r - \frac{(m_{ir}+m_{jr})^2\sigma^2}{2}} \right. \\ \left. + 2 \sum_{i,j,s=1}^m \prod_{k=1}^n e^{(m_{ik}+m_{jk}+m_{sk})x_k + \frac{((m_{ik}+m_{jk})^2+m_{sk}^2)\sigma^2}{2}} \sum_{r=1}^n e^{-m_{sr}x_r - \frac{m_{sr}^2\sigma^2}{2}} \right\} \\ = I \left\{ \sum_{i,j,s}^m \prod_{k=1}^n e^{(m_{ik}+m_{jk}+m_{sk})x_k + \frac{((m_{ik}+m_{jk})^2+m_{sk}^2)\sigma^2}{2}} \right. \\ \left. \times \sum_{r=1}^n \left(-1 - e^{-(m_{ir}+m_{jr})x_r - \frac{(m_{ir}+m_{jr})^2\sigma^2}{2}} + 2e^{-m_{sr}x_r - \frac{m_{sr}^2\sigma^2}{2}} \right) \right\}$$

The last sum above clearly goes to $-n$ as $\sigma^2 \rightarrow +\infty$. Thus, for σ^2 large enough, we have $g'(1) < 0$ which implies $g(p) \geq g(1) = 0$ for p close to 1 from the left hand side. This completes the proof.

A.3.2 Sketch of Proof of Theorem 3.5

The proof follows a similar line of arguments in the proof of Theorem 2 and thus, we point out only the main differences. We need to verify $\mathbb{E}\mathcal{L}_{LL}(y^*, s(MS_\alpha(\tilde{X}))) \leq \mathbb{E}\mathcal{L}_{LL}(y^*, s(M\tilde{X}))$ for α close to and larger than 1.

With $\lambda = 1/\alpha$, one can show (as in Lemma 2) that

$$\mathbb{E} \sum_{i=1}^m e^{MS_\alpha(\tilde{X})} = \sum_{i=1}^m e^{\lambda \sum_{k=1}^n m_{ik} x_k + \lambda^2 \sigma^2 \sum_{k=1}^n m_{ik}^2 / 2}$$

and

$$\mathbb{E} \left(\sum_{i=1}^m e^{MS_\alpha(\tilde{X})} \right)^2 = \sum_{i=1}^m \sum_{j=1}^m e^{\lambda \sum_{k=1}^n (m_{ik} + m_{jk}) x_k + \lambda^2 \sigma^2 \sum_{k=1}^n (m_{ik} + m_{jk})^2 / 2}.$$

Next, one can establish similar steps of (20), (21), and (22) for the current case and eventually complete the proof.

A.3.3 Concentration of the errors

Linear layer. Both conditions in Theorem 1 are necessary and sufficient conditions and indicate implicit relations between the input, X , the denoising parameters, p, α , the weight of the split layer, W , and the added noise magnitude α . For the masking case, the coefficient of the linear term, p , which can be positive or negative depending on the noise scale σ , dominates MSE; see Figure 2 (b). However, for Theorem 1 (ii), from (11), we observe the MSE depends quadratically on the scaling factor $\frac{1}{\alpha}$, where $\alpha > 1$. Therefore, one can observe a quadratic relation between the scaling factor $\frac{1}{\alpha}$, and MSE in Figure 2(a).

Nonlinear layer. For nonlinear loss functions, this relation is more complicated to observe. For Theorem 2, the loss is $\mathcal{L}_{LL}(y^*, s(MR_p(\tilde{X})))$, which is given in equation (2) in the main paper (also, see equation (18) in the Appendix). In this scope, we show how the bound on the error, $\mathbb{E}[\mathcal{L}_{LL}(y^*, s(M\tilde{X})) - \mathcal{L}_{LL}(y^*, s(MR_p(\tilde{X})))]$, depends on σ^2 and $(1-p)$. Based on equation (18), the first term will be $-(1-p)(MX)_{i^*}$, which is linear in $(1-p)$. The next term we need to consider is $\log \left(\mathbb{E}[\sum_{i=1}^m e^{(MR_p(\tilde{X}))_i}] \right) - \log \left(\mathbb{E}[\sum_{i=1}^m e^{(MX)_i}] \right)$. By directly manipulating the expression in (15) for p and $p = 1$ we find this quantity approximately is

$$\sum_{i=1}^m e^{\sum_{k=1}^n m_{ik} x_k} \left\{ (p^n - 1) + \sigma^2 p^n \frac{\sum_{k=1}^n m_{ik}^2}{2} + \text{Higher order terms} \right\} + O(1-p).$$

When the noise is not too large, say, $\sigma^2 \frac{\sum_{k=1}^n m_{ik}^2}{2} < 1$, we can observe that the bound is approximately linear in the variance of noise, σ^2 . One can obtain a similar observation for Theorem 3 as well.

A.4 Differential Privacy (DP)

We start by defining differential privacy.

Definition A.6. Dwork et al. (2014) A random mechanism, $\mathcal{K} : \mathcal{D} \rightarrow \mathbb{R}^m$ is (ϵ, δ) -differentially private if for all adjacent inputs, $D, D' \in \mathcal{D}$, with Hamming distance, $d(D, D') = 1$, and all possible output, $\mathcal{O} \in \mathbb{R}^m \in \mathcal{B}(\mathbb{R}^m)$ such that

$$P[\mathcal{K}(D) \in \mathcal{O}] \leq e^\epsilon P[\mathcal{K}(D') \in \mathcal{O}] + \delta,$$

where $P[\cdot]$ refers to the probability associated with the random mechanism \mathcal{K} and $\mathcal{B}(\mathbb{R}^m)$ is Borel sets in \mathbb{R}^m .

We also need the general theorem that says, any differentially private mechanism, $\mathcal{K} : \mathcal{D} \rightarrow \mathcal{O}$ is further differentially private if it is transformed by an arbitrary postprocessing function, deterministic or random; see Theorem 3.7 in the main paper.

Finally, if perform multiple computations of the random mechanism, \mathcal{K} on the same dataset, D , that is, we make T such passes on D , then the privacy guarantee degrades. We quote the advanced composition theorem from Dwork et al. (2010) for such mechanisms.

Theorem A.7. Dwork et al. (2010) Let $\mathcal{K} : \mathcal{D} \rightarrow \underbrace{\mathcal{O} \times \mathcal{O} \cdots \mathcal{O}}_{T\text{-times}}$ be an T -fold adaptive composition of (ϵ, δ) -DP mechanisms. Then \mathcal{K} is $(\epsilon', T\delta + \delta')$ -DP for $\epsilon' = \epsilon \sqrt{2T \ln(\delta'^{-1})} + T\epsilon(e^\epsilon - 1)$, for all $\delta' > 0$.

A.4.1 DP of the gradient during backpropagation

Setup. Let $\{(X_i, y_i^*)\}_{i=1}^N$ be training data points. Let the k^{th} layer of an L layer DNN be X_i^k , let Φ be a differentiable activation function, and let M_k^t be the weight matrix for the k^{th} layer at iteration t . By this convention, $X_i = X_i^0$. At $t = 0$, we have

$$X_i^j = \Phi_j(M_j^0 X_i^{j-1}), \quad y_i^j = M_j^0 X_i^{j-1}, \quad j = 1, \dots, L. \quad (23)$$

For the noisy split neural network with post-processing, let the split happen at the $(l-1)^{\text{th}}$ layer (so, the cut layer is the $(l-1)^{\text{th}}$ layer). With the notations above, we have:

$$\begin{cases} X_i^j = \Phi_j(M_j^0 X_i^{j-1}), \quad y_i^j = M_j^0 X_i^{j-1}, \quad j = 1, \dots, l-1, \\ \tilde{X}_i^{l-1} = X_i^{l-1} + \Delta, \tilde{X}_i^l = \Phi_l(M_l^0 h_D(\tilde{X}_i^l)), \tilde{y}_i^l = M_l^0 h_D(\tilde{X}_i^l), \\ \text{and } \tilde{X}_i^k = \Phi_k(M_k^0 \tilde{X}_i^{k-1}), \tilde{y}_i^k = M_k^0 \tilde{X}_i^{k-1}, k = l+1, \dots, L. \end{cases} \quad (24)$$

In our experiments, we use the regular backpropagation formula in our noisy split network training, which we formalize in the next Proposition.

Proposition A.8. *With the notations above, for a noisy split network with post-processing, during training, one can use the regular backpropagation algorithm by substituting: (i) $y_i^k = \tilde{y}_i^k, X_i^k = \tilde{X}_i^k$ for all subsequent $k = L-l+1, \dots, L$ and (ii) $y_i^r = y_i^r, X_i^r = X_i^r$ for all $r = 1, 2, \dots, l-1$, before the split, and $y_i^k = \tilde{y}_i^k$, for $k = L-l+1, \dots, L$ after the split.*

Define the sets, $S \subseteq \mathbb{R}^m$ and S^c as follows:

$$\begin{cases} S := \{z : p(z) > e^\epsilon p(z + V(D) - V(D'))\}, \\ S^c := \{z : p(z) \leq e^\epsilon p(z + V(D) - V(D'))\}, \end{cases} \quad (25)$$

Proposition A.9. *Let $\epsilon, \delta > 0$, and let a random mechanism $\mathcal{K} : D \rightarrow \mathbb{R}^m$ be defined as in (3). Then there exists a bound Δ_1 such that, for any two adjacent datasets, D and D' , when $\|V(D) - V(D')\| \leq \Delta_1$, we have that the random variable Z will satisfy $P[\omega : p(Z(\omega)) > e^\epsilon p(Z(\omega) + V(D) - V(D'))] < \delta$.*

The above Proposition can be verified as follows. Because, for two large enough datasets, D and D' , we can make let $\Delta := \|V(D) - V(D')\|$ small. Using Taylor expansion, we have

$$\begin{aligned} & p(z) - e^\epsilon p(z + V(D) - V(D')) \\ &= p(z) - e^\epsilon (p(z) + \nabla p(z)^\top (V(D) - V(D')) + o(\Delta^2)) \\ &\approx (1 - e^\epsilon) p(z) + O(\Delta) \leq 0. \end{aligned}$$

Here the last inequality is achieved by choosing small Δ_1 .

Theorem A.10. *Let a random mechanism, $\mathcal{K} : D \rightarrow \mathbb{R}^m$ as defined in equation 3 obey Proposition A.9. Then for ~~some~~any (ϵ, δ) , one can choose Δ_1 small enough such that \mathcal{K} is (ϵ, δ) -DP.*

Proof. Note that, $P[\mathcal{K}(D) \in \mathcal{O}] = P[V(D) + z \in \mathcal{O}] = P[z \in \mathcal{O} - V(D)] \stackrel{\mathcal{O}' := \mathcal{O} - V(D)}{=} P[z \in \mathcal{O}']$, where \mathcal{O}' is a shifted output set. We split the set \mathcal{O}' into two disjoint sets, $\mathcal{O}' \cap S$ and $\mathcal{O}' \cap S^c$. Therefore,

$$\begin{aligned} P[\mathcal{K}(D) \in \mathcal{O}] = P[z \in \mathcal{O}'] &= P[z \in ((\mathcal{O}' \cap S) \cup (\mathcal{O}' \cap S^c))] \\ &= P[z \in (\mathcal{O}' \cap S)] + P[z \in (\mathcal{O}' \cap S^c)] \\ &\stackrel{\mathcal{O}' \cap S \subseteq S}{\leq} P[z \in S] + P[z \in (\mathcal{O}' \cap S^c)] \\ &\stackrel{\text{Proposition A.9}}{<} \delta + P[z \in (\mathcal{O}' \cap S^c)]. \end{aligned} \quad (26)$$

Model & Dataset	Split Config. (denoted by)	Layer Size
CNN on MNIST	2×Conv2d - FC FC - Loss	256
	2×Conv2d FC - FC - Loss	12544
MLP on IMDB	Embedding - FC FC - Loss	16
	Embedding FC - FC - Loss	4096
ResNet-20 on CIFAR10	Conv2d - 3×ResBlock FC - Loss	256
ResNet-18 on CIFAR100	Conv2d - 4×ResBlock FC - Loss	512
RNN on Names	Embedding - RNN FC - Loss	256
ResNet-50 on ImageNet1K	Conv2d - 4×ResBlock FC - Loss	512
ALBERT-base-v2 on Amazon Reviews	12×Encoder FC - Loss	768

Table 1: Model split configurations and split layer sizes.

We also have

$$\begin{aligned}
P[z \in (\mathcal{O}' \cap S^c)] &= \int_{z \in \mathcal{O}' \cap S^c} p(z) dz \stackrel{\text{By equation 25}}{\leq} e^\epsilon \int_{z \in \mathcal{O}' \cap S^c} p(z + V(D) - V(D')) dz \\
&\stackrel{\mathcal{O}' \cap S^c \subseteq \mathcal{O}'}{\leq} e^\epsilon \int_{z \in \mathcal{O}'} \underbrace{p(z + V(D) - V(D'))}_{=u} dz \\
&= e^\epsilon \int_{u \in \mathcal{O} - V(D')} p(u) du \\
&= e^\epsilon \int_{z + V(D') \in \mathcal{O}} p(z) dz \\
&= e^\epsilon P[V(D') + z \in \mathcal{O}] \\
&= e^\epsilon P[\mathcal{K}(D') \in \mathcal{O}]. \tag{27}
\end{aligned}$$

Combining equation 26 and equation 27, we get the result. \square

Let $g_B^t(D)$ and $\tilde{g}_B^t(D)$ be two gradient vectors computed on the training dataset D over a minibatch B at iteration t without and with noise injected. Based on Proposition A.8 we have:

$$\begin{cases} g_B^t(D) = g(y_B^L(D), y_B^{L-1}(D), y_B^{L-2}(D), \dots, y_B^1(D)). \\ \tilde{g}_B^t(D) = g(\tilde{y}_B^L(D), \dots, \tilde{y}_B^L(D), y_B^{L-1}(D), \dots, y_B^1(D)). \end{cases}$$

Define $Z := \tilde{g}_B^t(D) - g_B^t(D)$ be a random vector. Hence,

$$\mathcal{K}_{BP}(D) := \tilde{g}_B^t(D) = g_B^t(D) + Z, \tag{28}$$

where $Z = G(\xi, \beta)$ is a random variable with probability density function $p(\tilde{z} \in \mathcal{O}) = p((\xi, \beta) \in G^{-1}(\mathcal{O}))$. In our case, we use masking and scaling as a postprocessing function, $h_D(\cdot)$ after the Gaussian noise injection. The random variable, $\xi \sim \mathcal{N}(0, \sigma I)$ is continuous. The mask, R_p is a random matrix of 1 and 0 with identical and independently distributed entries, $(R_p)_{ij} \sim \text{Bernoulli}(p)$, a discrete distribution. For scaling, S_α is an elementwise scaling operator. Therefore, for masking, $\tilde{y}_i^l = M_i^0 R_p(\tilde{X}_i^l)$, and the entries of $R_p(\tilde{X}_i^l) = X_i^{l-1}(D) + \Delta$ or 0, based on $(R_p)_{ij} \sim \text{Bernoulli}(p)$. On the other hand, for scaling, $\tilde{y}_i^l = M_i^0 S_\alpha(\tilde{X}_i^l)$ and the entries of $S_\alpha(\tilde{X}_i^l) = \frac{1}{\alpha}(X_i^{l-1}(D) + \Delta)$. Therefore, based on Theorem A.10, this mechanism is also differentially private.

B Addendum to the Numerical Results

Due to limited space, we were unable to discuss many experimental details as well as many results in Section 4 of the main paper. We discuss them here in detail.

Table 2: SplitNN setup and training hyper-parameters

Model	Dataset	Optimizer	Batch size	Epoch	lr	Weight decay
CNN	MNIST	SGD	64	4	0.1	0
ResNet-20	CIFAR-10	SGD-M	128	160	0.1	1e-4
ResNet-18	CIFAR-100	SGD-M	128	200	0.1	5e-4
MLP	IMDB	Adam	64	2	0.01	0
LSTM	Names	SGD	800	150	2	0
ALBERT-base-v2	Amazon Reviews	AdamW	256	10	5e-5	1e-2
ResNet-50	ImageNet1K	SGD	256	90	0.1	1e-4

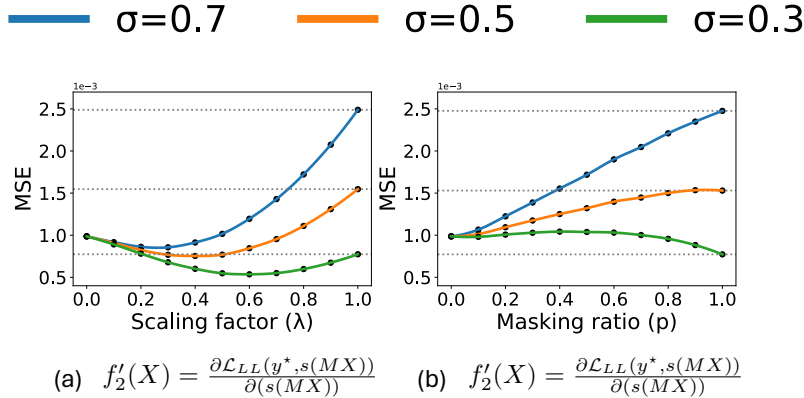


Figure 6: **Backward simulation.** Simulation of how scaling factor ($\lambda = \frac{1}{\alpha}$) and masking ratio (p) influence the estimation error (MSE) under different noise levels (σ) for linear (f_1) and nonlinear functions (f_2, f'_2). The backpropagation errors are essential during the training as we use them together with forward IRs to directly compute the gradients. By taking the derivative of the loss function w.r.t the IRs, we obtain the simulation of the MSEs for the backpropagation errors. Similar to the forward pass, scaling and masking, can lower the estimation error during the backward pass, especially when the noise level is relatively high.

B.1 Laplace mechanism

The Laplace Distribution (centered at 0) with scale b is the distribution with probability density function:

$$\text{Lap}(x | b) = \frac{1}{2b} \exp\left(-\frac{|x|}{b}\right)$$

Here, we consider the Laplace mechanism to protect the input vector X . Simulation results (Figure 7) show that our denoising methods can also decrease the estimation error caused by Laplace mechanism during forward and backward pass. However, in the real split learning task (see Table 3), our denoising methods are less effective for large Laplacian noise $b = 0.7$, compared with $\sigma = 0.7$ in Gaussian mechanism. More detailed investigation is left for future work.

B.2 Split learning result on CIFAR-100

We provide results on the CIFAR-100 dataset with ResNet-18 in Table 5. As shown in the table, both our denoising techniques achieve higher accuracy than simple learning rate tuning.

B.3 Understanding the scaling operation when gradient scale impact is eliminated

To further understand the scaling operations, we run the same MNIST experiment with two Adam optimizers separately for the client and server. The results in Table 6 demonstrate that the efficacy of scaling operation

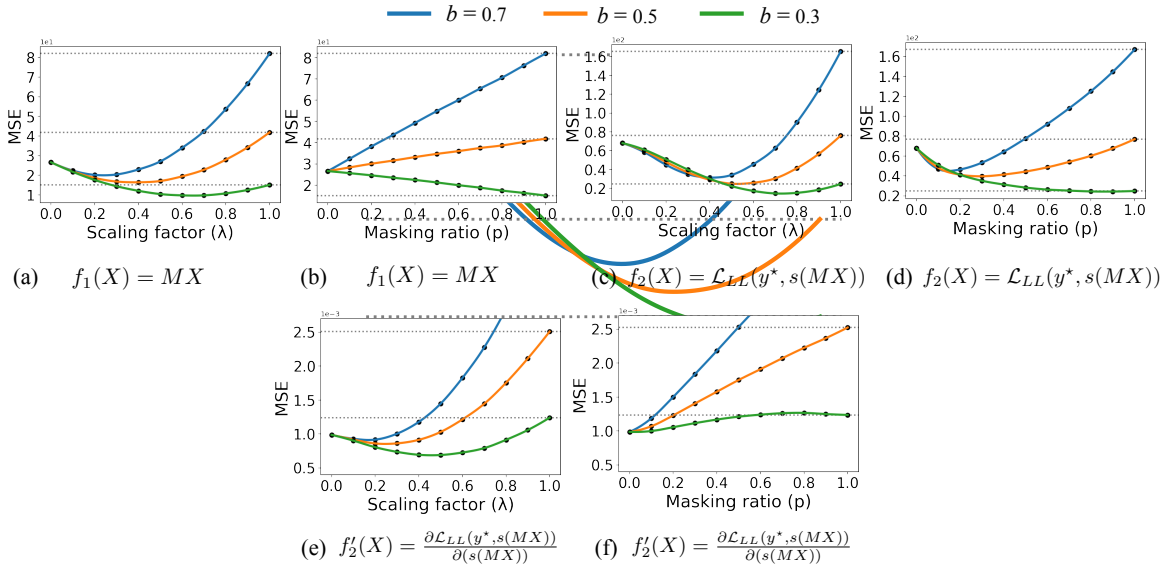


Figure 7: Simulation of how scaling factor ($\lambda = \frac{1}{\sigma}$) and masking ratio (p) influence the estimation error (MSE) under different Laplacian noise levels (b) for linear and nonlinear cases. Plots (a)–(d) are the linear layer and nonlinear layer during the forward pass, while (e)-(f) are the derivatives of the nonlinear layer during the backward pass.

Table 3: Denoising performance by using Laplacian noise in split learning for MNIST classification task (same experiment setting as Figure 3a). We fine-tune hyperparameters λ and p for different Laplacian noise scales $b = 0.3, 0.5, 0.7$. Compared with the Gaussian mechanism, split learning suffers more from Laplacian noise injection.

b	Best acc. (%)	$\lambda=0.1$	$\lambda=0.2$	$\lambda=0.4$	$\lambda=0.6$	$p=0.1$	$p=0.2$	$p=0.4$	$p=0.6$
0	98.96 (± 0.13)	-	-	-	-	-	-	-	-
0.3	92.64 (± 0.11)	95.66 (± 0.25)	94.49 (± 0.31)	92.16 (± 0.38)	90.93 (± 0.49)	98.19 (± 0.67)	98.55 (± 0.62)	98.32 (± 0.17)	95.54 (± 0.21)
0.5	38.30 (± 0.27)	94.58 (± 0.18)	93.44 (± 0.27)	89.11 (± 0.53)	85.10 (± 0.35)	96.98 (± 0.39)	97.48 (± 0.84)	95.17 (± 0.31)	89.01 (± 0.37)
0.7	16.62 (± 0.10)	21.44 (± 0.13)	23.49 (± 0.58)	20.52 (± 0.34)	14.71 (± 0.52)	12.85 (± 0.27)	23.62 (± 0.45)	18.42 (± 0.49)	15.58 (± 0.19)

still exists even when gradient scale impact is eliminated by Adam’s updating rule. If we compare our scaling method against learning rate tuning, the accuracy gain should be from 92.80% to 98.14%.

Learning rate	0.001	0.005	0.01	0.05	0.1
Top-1 Acc. (%)	87.68	92.67	81.21	diverge	diverge
Weight decay	0.01	0.05	0.1	0.2	0.4
Top-1 Acc. (%)	diverge	diverge	diverge	87.15	77.78
Dropout	0.1	0.2	0.4	0.6	0.8
Top-1 Acc. (%)	diverge	diverge	diverge	diverge	diverge
Masking	0.1	0.2	0.4	0.6	0.8
Top-1 Acc. (%)	98.31	98.62	diverge	diverge	diverge
Scaling*	0.1	0.2	0.4	0.6	0.8
Top-1 Acc. (%)	98.10	96.06	90.25	diverge	diverge

Table 4: Comparison of tuning various hyper-parameters in noise injected SplitNN training at a fixed noise level ($\sigma = 0.7$) for MNIST classification. * means co-optimization with weight decay.

Table 5: Top-1 Accuracy (%) of split learning using ResNet-18 on CIFAR-100 dataset with noise injection level ($\sigma = 0.7$). The baseline achieves 75.60% Top-1 accuracy using SGD-Momentum (m=0.9) with an initial learning rate of 0.1, and weight decay $5e^{-4}$.

Learning rate	0.001	0.005	0.01	0.05	0.1
Top-1 Acc. (%)	53.11	68.93	61.54	diverge	diverge
Masking (lr=0.1)	0.1	0.2	0.4	0.6	0.8
Top-1 Acc. (%)	60.49	72.38	63.31	52.97	diverge
Scaling (lr=0.1)	0.1	0.2	0.4	0.6	0.8
Top-1 Acc. (%)	72.21	71.68	68.14	57.54	diverge

B.4 Split learning on large datasets

We use two large-scale datasets, Amazon Reviews McAuley & Leskovec (2013) for sentiment analysis and ImageNet1K Deng et al. (2009) for image classification tasks, and investigate how the proposed denoising strategies perform in large-scale, challenging datasets. For the experiments on the Amazon Reviews dataset, we use a pre-trained ALBERT-base-v2 Lan et al. (2020); for the ImageNet1K experiments, we use ResNet50; see Table 7 for the results. We provide the split configurations and the training hyperparameters for these experiments in Tables 1 and 2, respectively. As the ALBERT-base-v2 was a pre-trained model, we fine-tuned it on the Amazon Reviews dataset, and observed that noise injections or denoising strategies, such as masking and scaling, had an insignificant effect on the baseline performance. Noise injections do not degrade the performance, and denoising strategies do not improve them either. On the other hand, the performance of ResNet50 on ImageNet1K was heavily impacted by the noise injection. E.g., a noise injection of $\sigma = 0.5$ renders a test accuracy of 1.92, which is 97% lower than the baseline accuracy. When we apply the denoising strategies to the noise-injected IRs, at the same noise level $\sigma = 0.5$, the scaling strategy with $\lambda = 0.1$ and masking strategy with $p = 0.2$ recover performance comparable to the baseline.

B.5 Experiments on Split Position

We investigated the network behavior in a [two-party split learning](#) setup and experimented with different [positions of the split layer in a network](#). For this, we selected the configurations of MLP on the IMDB dataset and ResNet20 on the CIFAR10 dataset with the highest noise-level, $\sigma = 0.7$; see Table 8 for the results. [We observe a performance degradation when the position of the split layer is early in the network. However, the proposed denoising strategies successfully improve performance on top of the noisy IRs, even though the recovery to the baseline accuracy becomes difficult in such cases.](#) We also observe that for MLP architectures, the scaling strategy is more effective for denoising, while the masking strategy is more effective for ResNet architectures.

B.6 Computational overhead of the postprocessing functions

We measured the computational overhead introduced by the denoising techniques on both CPU and GPU. The results are shown in Table 9. The computational overhead of scaling and masking is negligible compared to the training computation.

Table 6: Top-1 Accuracy(%) of split learning on MNIST dataset with noise injection level ($\sigma = 0.7$). Use two Adam optimizers separately for the client and server. The Adam baseline (lr=1e-3) achieves 98.95% top-1 accuracy.

Learning rate	1e-6	1e-5	1e-4	1e-3	0.1
Top-1 Acc. (%)	83.96	92.80	90.13	diverge	diverge
Scaling ratio (lr=1e-4)	0.1	0.2	0.4	0.6	0.8
Top-1 Acc. (%)	97.19	97.94	98.14	96.03	91.75

Table 7: Performance of scaling (λ) and masking (p) at different noise levels (σ) for large-scale datasets, ImageNet-1K, and Amazon Reviews Full.

Task	Noise level (σ)	Best acc. (%)	$\lambda=0.1$	$p=0.2$
ResNet50-ImageNet	0	74.85	-	-
	0.3	31.18	74.26	73.79
	0.5	1.92	72.93	73.07
ALBERT-base-v2-Amazon Reviews	0	65.19	-	-
	0.3	65.15	65.12	65.15
	0.5	65.18	65.16	65.13

Table 8: Performance of scaling (λ) and masking (p) for different splits of the networks.

Task	Splits	σ	Best acc. (%)	$\lambda=0.1$	$\lambda=0.2$	$p=0.1$	$p=0.2$
MLP-IMDB	-	0	85.53	-	-	-	-
	Embedding - FC FC - Loss	0.7	76.28	83.25	82.35	82.82	83.41
	Embedding FC - FC - Loss	0.7	69.08	73.61	72.91	64.95	66.12
ResNet20-CIFAR10	-	0	91.76	-	-	-	-
	Conv2d - 3×ResBlock FC - Loss	0.7	80.69	86.69	87.16	89.07	89.48
	Conv2d - 2×ResBlock 1×ResBlock - FC - Loss	0.7	66.16	35.53	38.22	85.01	86.95

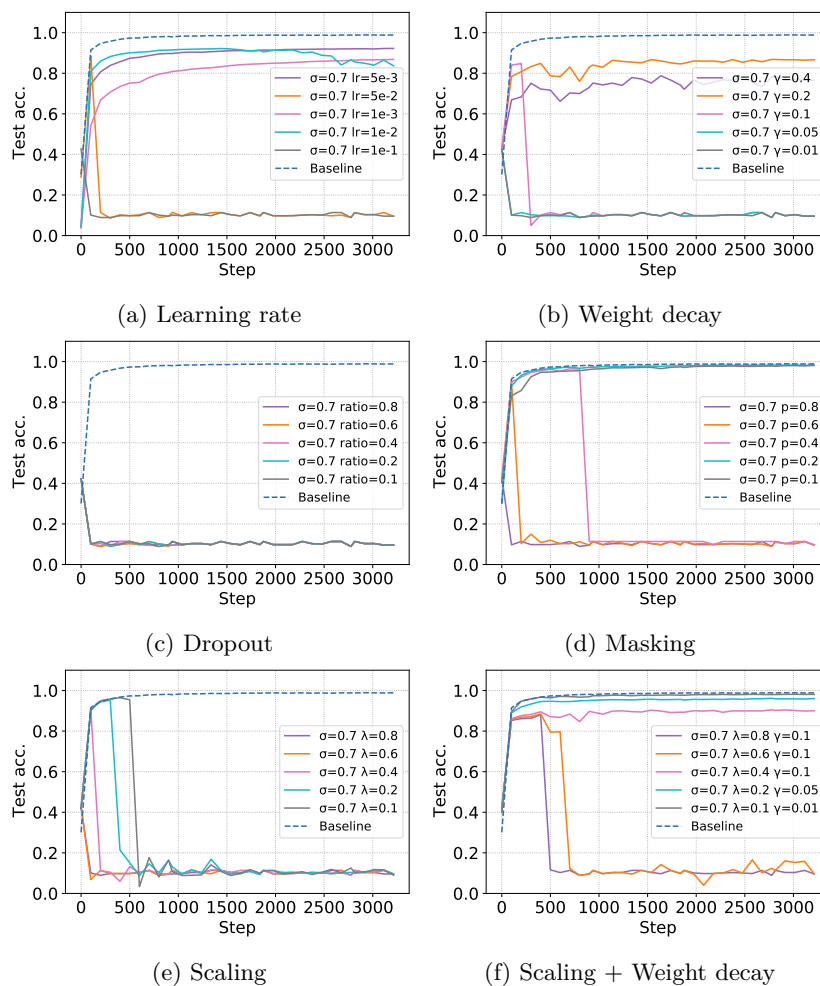
Figure 8: Comparison of tuning various hyper-parameters in noise-injected split learning at a fixed noise level ($\sigma = 0.7$) for MNIST classification task.

Table 9: Run time profiling for one mini-batch training of CNN on MNIST dataset. GPU: NVIDIA A100-80GB GPU. CPU: Intel Xeon Platinum 8260 CPU @ 2.40GHz.

Hardware	Baseline	Noise injection only	Noise injection w. masking	Noise injection w. scaling
GPU	1.54 ms	1.88 ms	1.91 ms	1.92 ms
CPU	22.16 ms	22.27 ms	23.40 ms	23.19 ms

Table 10: Hyper-parameter tuning for scaling (λ) and masking (p) at different noise level (σ). Results are obtained by running the experiment 3 times with different random seeds. We record the best test accuracy during the training instead of the final accuracy.

Task	σ	Best acc. (%)	$\lambda=0.1$	$\lambda=0.2$	$\lambda=0.4$	$\lambda=0.6$	$p=0.1$	$p=0.2$	$p=0.4$	$p=0.6$
CNN-MNIST	0	98.96 (± 0.13)	-	-	-	-	-	-	-	-
	0.3	98.46 (± 0.07)	97.63 (± 0.27)	97.13 (± 0.23)	96.07 (± 0.10)	95.42 (± 0.17)	98.93 (± 0.14)	98.88 (± 0.19)	98.86 (± 0.11)	98.77 (± 0.09)
	0.5	90.99 (± 0.38)	97.59 (± 0.20)	97.07 (± 0.63)	95.87 (± 0.09)	94.62 (± 0.94)	98.78 (± 0.15)	98.84 (± 0.16)	98.74 (± 0.30)	94.36 (± 1.13)
	0.7	81.85 (± 0.77)	97.11 (± 0.15)	96.30 (± 0.36)	90.95 (± 0.22)	88.88 (± 0.28)	98.31 (± 0.38)	98.62 (± 0.23)	96.67 (± 0.14)	90.51 (± 1.09)
ResNet20-CIFAR10	0	91.76 (± 0.28)	-	-	-	-	-	-	-	-
	0.3	90.98 (± 0.23)	89.15 (± 0.51)	90.13 (± 0.95)	90.67 (± 0.49)	90.84 (± 0.43)	88.69 (± 0.80)	89.54 (± 0.57)	90.30 (± 0.26)	90.15 (± 0.31)
	0.5	89.72 (± 0.49)	89.93 (± 0.52)	90.50 (± 0.74)	90.33 (± 0.72)	89.97 (± 0.62)	88.21 (± 0.50)	89.55 (± 0.73)	89.98 (± 0.98)	89.65 (± 1.10)
	0.7	82.03 (± 0.76)	88.88 (± 0.74)	87.95 (± 0.13)	87.21 (± 0.79)	85.80 (± 0.88)	88.45 (± 0.90)	89.15 (± 1.16)	88.52 (± 1.29)	87.60 (± 1.41)
MLP-IMDB	0	85.53 (± 0.18)	-	-	-	-	-	-	-	-
	0.3	85.42 (± 0.30)	85.85 (± 0.63)	85.49 (± 0.17)	84.72 (± 0.58)	85.47 (± 0.03)	85.49 (± 0.33)	85.54 (± 0.55)	85.64 (± 0.51)	85.21 (± 0.74)
	0.5	84.85 (± 0.63)	85.44 (± 0.68)	85.35 (± 0.84)	84.06 (± 0.58)	84.55 (± 0.72)	85.55 (± 0.69)	86.00 (± 0.36)	85.18 (± 0.62)	85.92 (± 1.22)
	0.7	64.91 (± 1.71)	84.24 (± 0.38)	84.24 (± 0.94)	82.83 (± 0.36)	80.90 (± 0.71)	85.11 (± 0.40)	85.08 (± 0.30)	83.27 (± 1.38)	84.88 (± 1.03)
LSTM-Names	0	81.24 (± 0.25)	-	-	-	-	-	-	-	-
	0.3	82.31 (± 0.81)	83.76 (± 0.58)	82.35 (± 0.27)	81.17 (± 0.31)	80.51 (± 0.59)	80.52 (± 0.36)	82.05 (± 0.40)	81.63 (± 0.08)	82.23 (± 0.83)
	0.5	56.91 (± 1.42)	82.17 (± 0.64)	81.70 (± 0.78)	81.56 (± 0.45)	81.43 (± 0.95)	80.13 (± 0.52)	82.54 (± 1.03)	82.04 (± 1.21)	82.57 (± 0.06)
	0.7	47.65 (± 1.97)	81.56 (± 0.34)	80.87 (± 0.58)	81.07 (± 0.81)	66.68 (± 0.57)	79.35 (± 0.35)	81.15 (± 0.75)	80.40 (± 0.75)	46.59 (± 1.33)

B.7 Feature-space hijacking attack (FSHA) and our post-processing techniques

Threat model. We assume that the attacker has no information on the architecture of the client’s model and its weights. However, the attacker knows a public dataset that captures the same domain as the clients’ training sets. For example, if the model is trained on face images, then the public dataset is composed of face images as well. This assumption is more realistic and less restrictive than the ones adopted in other works Vepakomma et al. (2019)Vepakomma et al. (2018b), where the attacker is assumed to have direct access to leaked pairs of intermediate results and private training data.

In the FSHA Pasquini et al. (2021) attack, the attacker (e.g., the server) can hijack the client’s learning process and learn an inverse version of the client’s model. During the inference, the attacker can recover the client’s raw data by using the output of the client. In this work, we showed that the masking operator simultaneously improves the SplitNN training and, in the meantime, decreases the efficacy of the FSHA attack. Our intuition is that the denoising effect depends on the specific application, which is a function applied to the noisy input, $X + \Delta$. If the function’s goal is to identify each value of X , such as reconstructing an image in an FSHA attack, then denoising cannot help too much. However, if the goal is to get a more accurate estimation on some statistical metrics of X , such as the mean, norm of X , then it is possible to have an evident denoising improvement.

Table 11: We provide the privacy bounds for one single forward pass during the SplitNN training, for various noise levels used in our work, without denoising. We compare it with two state-of-the-art results for private split learning.

Method	Model & Dataset	DP mechanism	Inference	Training	Noise scale	DP bounds
Titcombe et al. 2021	2D CNN on MNIST	Laplace	✓		0.1, 0.5, 1.0	N/A
Abuadba et al. 2020	1D CNN on medical data	Laplace		✓	N/A	$\epsilon = 1, 3, 5, 7, 10$
Our work (w/o sampling amplification)	2D CNN on MNIST	Gaussian	✓	✓	0.3, 0.5, 0.7	$\epsilon = (260, 150, 110)*2, \delta = 1e-5$
	ResNet on CIFAR10	Gaussian	✓	✓	0.3, 0.5, 0.7	$\epsilon = (264, 152, 112)*2, \delta = 1e-5$
	MLP on IMDB	Gaussian	✓	✓	0.3, 0.5, 0.7	$\epsilon = (168, 96, 72)*2, \delta = 1e-5$
	LSTM on Names	Gaussian	✓	✓	0.3, 0.5, 0.7	$\epsilon = (9.2, 5.3, 3.9)*2, \delta = 1e-5$
Our work (w/o sampling amplification)	2D CNN on MNIST	Laplace		✓	0.3, 0.5, 0.7	$\epsilon = (53.3, 32, 22.8)*2$
	ResNet on CIFAR10	Laplace		✓	0.3, 0.5, 0.7	$\epsilon = (53.3, 32, 22.8)*2$
	MLP on IMDB	Laplace		✓	0.3, 0.5, 0.7	$\epsilon = (13.3, 8, 5.7)*2$
	LSTM on Names	Laplace		✓	0.3, 0.5, 0.7	$\epsilon = (53.3, 32, 22.8)*2$

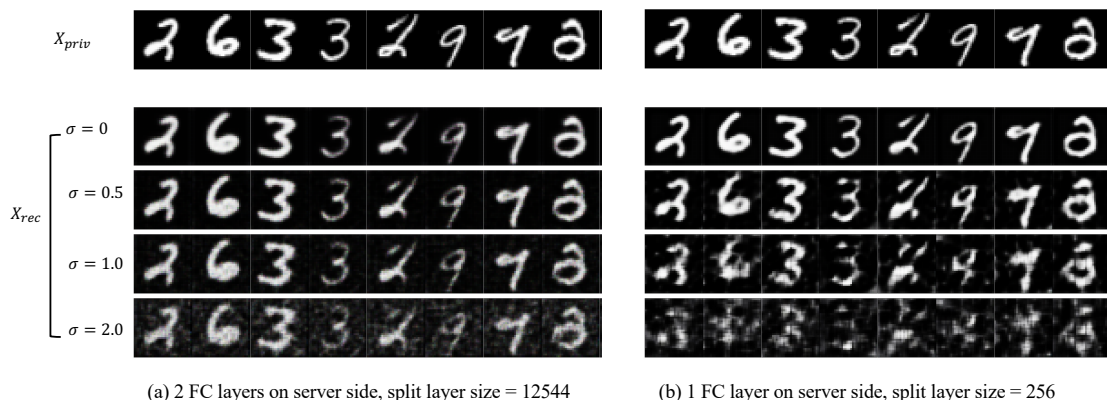


Figure 9: Private data recovery by FSHA in split learning on MNIST. X_{priv} : the original private data, X_{rec} : obtained by FSHA attack. We compare two different split learning settings: (a) split 2 FC layers on the server side (b) split 1 FC layer on the server side. The dimensions of the split layer are also different. We can see that by splitting more layers on the server side, it is more likely to reconstruct private training even when the noise level is relatively high ($\sigma = 1.0, 2.0$).

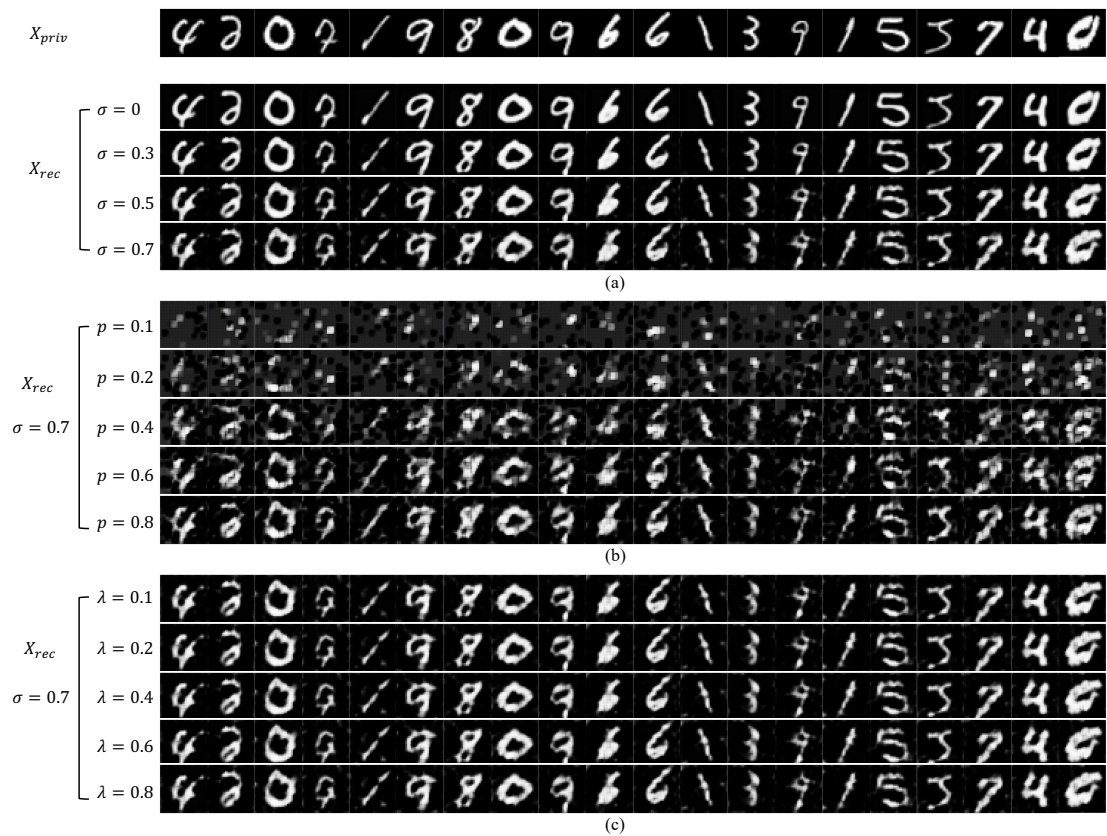


Figure 10: Private data recovery by FSHA in split learning on MNIST. X_{priv} : the original private data, X_{rec} : obtained by FSHA attack in various settings: (a) noise injection only, (b) noise injection + masking, (c) noise injection + scaling.



Figure 11: Private data recovery by FSHA in split learning on Fashion-MNIST. X_{priv} : the original private data, X_{rec} : obtained by FSHA attack in various settings: (a) noise injection only, (b) noise injection + masking, (c) noise injection + scaling.

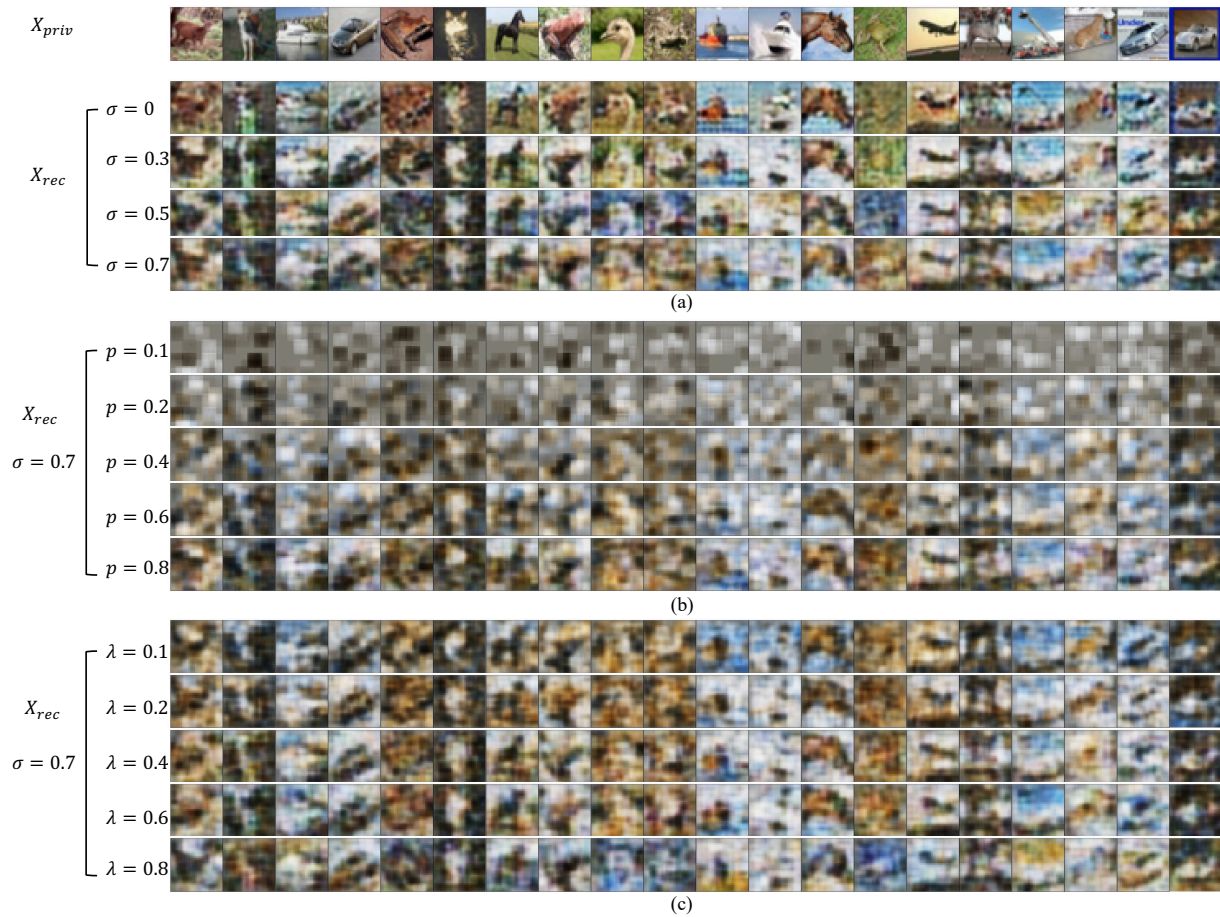


Figure 12: Private data recovery by FSHA in split learning on CIFAR-10. X_{priv} : the original private data, X_{rec} : obtained by FSHA attack in various settings: (a) noise injection only, (b) noise injection + masking, (c) noise injection + scaling.

B.8 DP budget

We provide the privacy bounds for one single forward pass during the SplitNN training in Table 11. By using the general composition Theorem, Theorem A.7 in the Appendix, we can calculate the total privacy budget for the entire training process. Although Theorem A.7 gives a theoretical formalization, in practice, if we use Theorem A.7 directly, it will result in a large privacy bound, which may not be practical. As argued in the paper DP-SGD, Abadi et al. found that even for local SGD training using Theorem A.7 would result in a large privacy bound and proposed a new accounting for local noisy SGD training. However, noisy SplitNN is a more complicated architecture, and DP-SGD analysis cannot be adopted here. Currently, privacy accounting for noisy SplitNN training remains an open problem. Improving the privacy accounting for split learning is not the primary focus of this work; instead, we want to show how denoising can improve noisy SplitNN accuracy.

C Limitations

Our denoising techniques work empirically on diverse datasets (MNIST, FMNIST, CIFAR-10, CIFAR-100, ImageNet1K, IMDB, Amazon Reviews, and Names) and across different network architectures (CNN, RNN, Transformer, and MLP). One of the potential drawbacks or limitations of the denoising techniques empirically is finding a good scaling or masking ratio. Another potential limitation could be that our proposed denoising techniques may not work for other loss functions. However, theoretically, we covered almost all the existing loss functions used for common DNN training; please see our discussion in the Appendix. Generalizing our theoretical claims to a broader class of nonlinear loss functions, such as sparse categorical cross-entropy, which is also rarely used in practice, requires further non-trivial investigation and is a scope for future research. Our present theoretical analyses in Section 3.1. and 3.2 consider the split layer at the pre-final layer of an L layer DNN; analysis of the split at an arbitrary i -th layer, along with the final loss function used for DNN training, requires much more mathematical rigor.